Nano Research Energy

ISSN 2791-0091 (print); 2790-8119 (online)
https://doi.org/10.26599/NRE.2025.9120210

Review Article

Electrolyte effects at solid–liquid interfaces in electrocatalysis: From fundamentals to electrolyte engineering

Xianwei Liu[1,§], Xianrong Zhang[1,§], Yuanqing Shen[1,§], Haikui Gao[1], Yuetong Wang[1], Xiaomin Han[1], Xulai Gong[1], Ruitian Kou[2], Jiaqi Liu[1], Canjie Zhang[1], Jiyao Liu[1], Linjie Zhao[1] (✉), Baoguang Mao[1] (✉), and Chuangang Hu[1] (✉)

[1] *State Key Laboratory of Organic-Inorganic Composites, Beijing Key Laboratory of Intelligent Design and Manufacturing for Hydrogen Energy Materials, College of Chemical Engineering, Beijing University of Chemical Technology, Beijing 100029, China*
[2] *Beijing Advanced Innovation Center for Soft Matter Science and Engineering, Beijing University of Chemical Technology, Beijing 100029, China*
[§] *Xianwei Liu, Xianrong Zhang, and Yuanqing Shen contributed equally to this work.*

Received: 7 October 2025 / **Revised:** 11 November 2025 / **Accepted:** 19 November 2025 / **Published date:** 17 December 2025

ABSTRACT

The universality and atomic-level structure of solid-liquid interfaces critically govern functionality across chemical, biological, and geological systems. In electrocatalysis, this interfacial structure dictates reaction thermodynamics and kinetics. However, fundamental understanding of structure-property relationships and their correlation with preferential reaction pathways remains incomplete. While conventional models emphasize adsorbate-surface covalent bonding and long-range electrode-electrolyte electrostatic interactions, emerging evidence highlights the significant impact of non-covalent adsorbate-electrolyte interactions on the electrical double layer (EDL) structure and electrocatalytic kinetics. Critically, both electrode and electrolyte co-determine catalytic performance. Despite advances in catalyst design, the electrolyte's role in modulating the local interfacial environment is inadequately understood, hindering optimization of activity, selectivity, and stability. Elucidating interfacial electrolyte effects is thus paramount, equaling the importance of intrinsic catalyst properties. This review commences by evaluating established and emerging theoretical frameworks describing the electrochemical solid-liquid interphase. Progressing to mechanistic insights, we decipher the role of electrolyte composition—specifically cation/anion speciation, concentration, and pH—in modulating the activity and selectivity of core electrocatalytic reactions. Critical assessment follows of state-of-the-art *operando* spectroscopic and scattering methodologies for resolving the dynamic evolution of buried interfaces. We conclude by delineating fundamental knowledge gaps and strategic research trajectories for electrolyte engineering to advance electrocatalytic microenvironments.

KEYWORDS

electrocatalysis, electrode-electrolyte interface, electrical double layer, electrolyte effects

1 Introduction

The solid-liquid interface plays an important role in various scientific fields and is crucial for understanding of the physical phenomena and interface structure [1–6]. This is particularly relevant in areas such as catalysis [7–9], crystal growth [10, 11], lubrication [12, 13], electrochemistry [14, 15], colloidal system [16, 17], and many biological reactions [18, 19]. Notably, the solid-liquid interface is the key to electrochemical processes that occur at the electrochemical boundary between the solid electrode and the liquid electrolyte [20]. To enable efficient conversion of electrical to chemical energy at this interface, it is essential to deeply understand its structure and properties, including the composition of electrode materials, the configuration of the double layer, and the characteristics of electrolytes [21]. The fundamental electrochemical interface reactions generally follow five key steps: (1) Mass transfer in the electrolyte. The transport of reactant molecules to the electrode surface. (2) Pre-surface transfer. The movement of reactant molecules near the electrode surface or within the adjacent electrolyte layer, including surface adsorption and chemical adsorption processes. (3) Electrochemical reaction. The transfer of electrons between the reactant molecules and the electrode surface, resulting in the generation of products. (4) Post-transfer process. The removal of reaction products from the electrode surface or the adjacent electrolyte layer, involving processes such as product desorption or further chemical transformations. (5) Formation of new phases and product transfer. For example, gas or solid, which then transfer from the electrode surface to the bulk solution [22, 23].

Address correspondence to Linjie Zhao, 2024700022@buct.edu.cn; Baoguang Mao, bgmao@buct.edu.cn; Chuangang Hu, chuangang.hu@mail.buct.edu.cn

By examining electrochemical processes at the solid-liquid interface, it becomes evident that many crucial reactions occur within the double layer [24, 25]. Traditionally, the understanding of electrochemical interfaces has focused on covalent interactions between adsorbates and solid electrode surfaces [26–28], as well as electrostatic interactions between electrolytes and electrode surfaces [29–32]. However, with ongoing research, it has become clear that non-covalent interactions between adsorbates and electrolytes also significantly affect the structure of the double layer and the kinetics progress of catalytic reactions [33–35]. In electrocatalytic reactions, achieving high catalytic performance depends on the synergistic interplay between catalyst materials and electrolytes. While the design and preparation of high-performance catalysts for various electrocatalytic reactions have made significant progress, the role of electrolytes in affecting the thermodynamics and kinetics progress of electrochemical reactions at solid-liquid interfaces remains unclear. Electrolytes greatly affect the local catalytic environment, playing a critical role in optimizing reaction pathways and regulating kinetic processes [36–38]. Experimental data suggest the presence of a barrier between catalytic reaction kinetics and thermodynamics in electrochemical systems. However, there is still a limited understanding of how electrolytes impact interface structures at the atomic and molecular levels. Therefore, to fully unlock the catalytic potential of electrochemical reactions, it is essential to emphasize the role of electrolytes and elevate their importance to the same level as that of the catalyst materials.

Herein, we summarize the influence of electrolytes on electrocatalytic activity and selectivity in different electrochemical reactions and advanced *in-situ* characterization techniques, which enable the construction of a dynamic and comprehensive picture of electrochemical processes. First, we discuss the current understanding of electrochemical solid-liquid interface and its model development. Secondly, we delve into the role of electrolytes on the activity of various electrocatalytic reactions. Next, the developed techniques for *in-situ* monitoring and characterization of electrochemical interfaces are introduced, which helps us to have a more intuitive understanding of the real-time dynamic changes of solid-liquid interfaces during electrochemical processes. Finally, we provide an outlook on the future development and challenges faced by electrolytes in various electrocatalytic reactions.

2 Fundamental principles of electrode-electrolyte interface

Due to the complex species interactions and energy exchange between catalysts and electrolytes, the electrochemical interface during electrocatalytic reactions is not a static entity but rather a dynamically evolving and broadened structure. Without a proper understanding of this interface at the atomic scale, it becomes challenging to fully grasp the fundamental properties of the solid-liquid interface. In the electrochemical process, the electrostatic interaction between the charged interface and counter-ions attracts ions with opposite charges from the bulk solution to the interface, while competing with the thermal effect that favors a more uniform ion distribution. This results in a non-uniform charge distribution along the normal direction of the interface, forming a strong interface electric field, often exceeding 10^8 V·cm^{-1} [39]. This intense electric field significantly influences catalyst surface fluctuations, charge transfer, ion distribution, solvent molecule orientation, and more complex interactions between them [40].

The discovery and development of the electrical double layer (EDL) span several decades (Fig. 1). In 1853, Helmholtz first identified that charged electrodes in the electrolyte attract ions with opposite charges, forming two layers at the electrode-electrolyte interface, now known as the Helmholtz model [41, 42]. This model treats the charged interface like a parallel plate capacitor, where one plate represents the charged surface, and the other corresponds to the closest hydrated counter-ion, forming the outer Helmholtz plane (OHP). However, the Helmholtz model overlooks factors such as ion diffusion, adsorption, and solvent-electrode interactions, assuming that EDL capacitance is constant and independent of electrode potential or ion concentration [43]. Gouy and Chapman later proposed the Gouy-Chapman model, introducing the concept of a diffusion layer and describing ion distribution via the Poisson-Boltzmann equation [44, 45]. This model suggests that ion concentration varies with distance from the electrode, and the potential decreases exponentially. While this was an improvement, the model assumes ions are point charges, which can approach the electrode surface infinitely under high polarization, which does not align with experimental data. In fact, ions are solvated and can only approach the electrode up to their solvation radius. The Debye-Hückel approximation, a linearized version of the Poisson-Boltzmann equation, is applicable in low-potential cases, though it is also used for nominally high-charged surfaces due to counter-ion effects [46]. Building on these models, Stern incorporated finite-sized ions and explained the reduced dielectric constant of water near the interface, creating the Gouy-Chapman-Stern (GCS) model [47]. This model includes a diffusion layer outside the OHP, accounting for ion shielding effects on surface charges. However, these mean-field models still have limitations, as they do not consider specific ion adsorption, which can alter local behavior at the interface. Graham suggested that certain ions or neutral substances could penetrate the Helmholtz layer, leading to the separation of inner and outer Helmholtz layers [43]. Further developments by Conway, Bockris, and Ammar introduced the role of water dipole properties [48], while Bockris, Devanathan, and Müller (BDM) refined the model by accounting for different dielectric constants in water layers [49], establishing a more comprehensive and widely accepted EDL model.

3 The influence of electrolytes on electrocatalytic reactions

As mentioned earlier, electrolytes are an indispensable component in EDL. They interact with the metal electrode surface through electrostatic forces in the outer Helmholtz layer, influencing the catalytic performance of electrochemical reactions. Additionally, electrolytes engage in non-covalent interactions with adsorbates, which affect the structure of double layer and the kinetics of catalytic reactions. A deep understanding of the role electrolytes play in electrocatalytic reactions is essential for gaining insight into the dynamic changes progress at solid-liquid interface during catalytic reactions and for developing effective strategies to enhance the performance of specific reactions. In this section, we will elaborate on the influence of electrolytes on the electrocatalytic activity, selectivity, and stability in different electrochemical reactions.

3.1 Electrocatalytic activity

3.1.1 *Hydrogen oxidation reaction*

The classical model of solid electrode-electrolyte interface

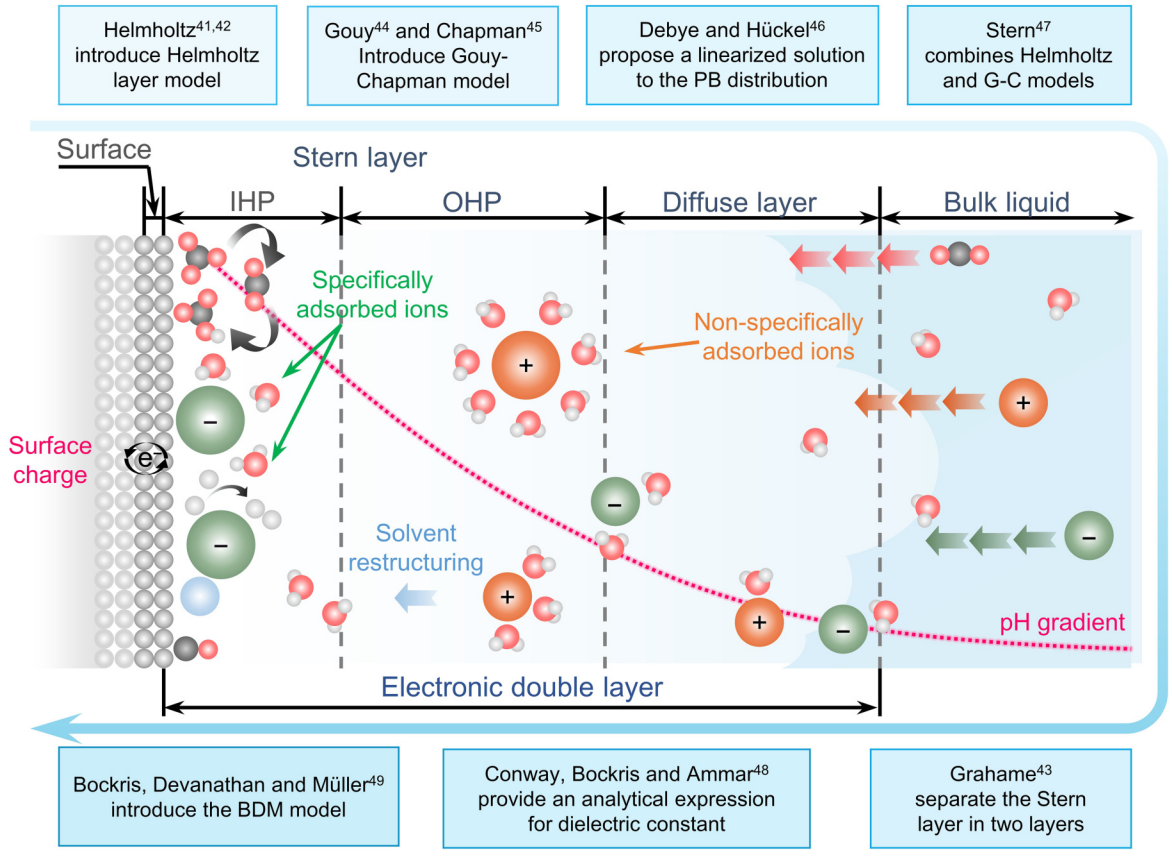

Figure 1 Classical mean-field theory of the electrical double layer and timeline.

primarily focuses on the covalent interaction between adsorbate and solid surface, as well as the long-range electrostatic interaction between electrolyte and metal electrode. However, the non-covalent interaction between adsorbate and electrolyte are equally crucial for understanding electrocatalytic trends. Markovic et al. investigated the role of alkali metal cations on electrocatalytic interfaces of Pt (111) and observed that these cations did not affect the region associated with underpotentially deposited hydrogen (H_{upd}) and the double-layer features, indicating no specific adsorption between the cations and the Pt electrode surface [50] (Figs. 2(a) and 2(b)). Conversely, in the region related to reversible adsorption of OH (OH_{ad}) species, the presence of Li^+ significantly enhanced the adsorption of OH_{ad}, forming OH_{ad}-$Li^+(H_2O)_x$. This increased OH coverage in the compact double layer reduced the number of Pt active sites, leading to slower reaction kinetics. This specific non-covalent interaction appears to increase in line with the hydration energy of the cations: $Li^+ > Na^+ > K^+ > Cs^+$.

Shao-Horn et al. further demonstrated, using classical molecular dynamics (MD) simulations, that the local solvation environment at the Pt (111) interface also follows cation-dependent effect at both pH 1 and pH 13 [51]. Structure-making cations (such as Li^+ and Na^+) retain their solvated shell at the electrical interface, while structure-breaking cations (such as Rb^+ and Cs^+) exhibit partial de-solvation and tend to aggregate on the surface. This cation-dependent interface structure was more pronounced at pH 13, where the negative surface charge was exhibited a systematic increase of up to 2 orders of magnitude in the sequence of $Cs^+ < Rb^+ < K^+ < Na^+ < Li^+$, with a corresponding decrease in the recombination energy according to Marcus-Hush-Chidsey (MHC) analysis.

However, a different conclusion was observed in the polycrystalline Pt system. Oezaslan et al. investigated the effect of alkali metal cations on the hydrogen oxidation reaction (HOR) activity based on polycrystalline Pt electrodes in alkaline media and found that Li^+ shifted the adsorption/desorption potentials of H_{upd} to lower values (~15 mV), compared to K^+ and Na^+ [52] (Fig. 2(c)). This observation aligns with Koper et al.'s findings on Pt (553) surfaces, where H_{upd} showed similar negative shift in the presence of monovalent cations [53] (Fig. 2(d)). The HOR on polycrystalline Pt increased in the order of $K^+ < Na^+ < Li^+$. This improvement is ascribed to the arrangement of water molecules controlled by the alkali metal cations, leading to non-covalent interactions between the hydrated cations and adsorbed hydrogen, which enhances the reaction kinetics in alkaline media, particularly with LiOH. These non-covalent interactions play a crucial role in improving the HOR activity, highlighting the importance of cation control in alkaline solutions as a regulatory parameter for electrocatalytic performance, though variations in catalyst structure may affect this regulation.

In addition to inorganic alkali metal cation, organic cations also impact HOR activity. Matanovic et al. investigated the role of organic cations on HOR using Pt/C in three types of 0.1 M alkaline electrolytes: tetramethylammonium hydroxide (TMAOH), tetrabutylammonium hydroxide (TBAOH) and tetrabutylphosphonium hydroxide (TBPOH) [54]. They found that organic cations specifically chemisorbed on the Pt surface, driving co-adsorption of hydroxide ions. TMA^+ exhibited stronger adsorption and affinity than TBA^+ and TBP^+, with hydroxide co-adsorption following the order $TMA^+ > TBA^+ > TBP^+$, leading to inhibited HOR activity (Figs. 2(e) and 2(f)).

Xu et al. further revealed that organic cations can induce the formation of long-range ordered structures in interfacial water

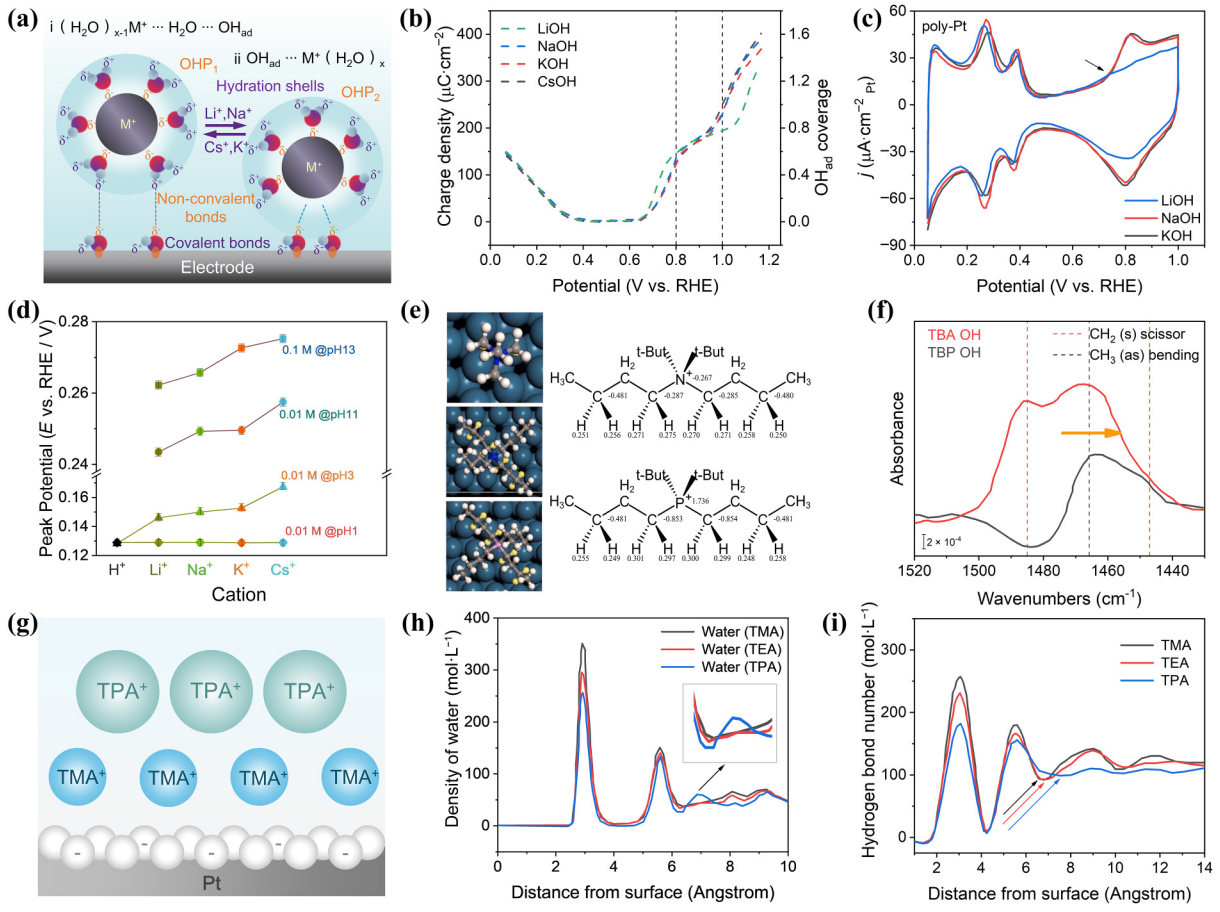

Figure 2 (a) Modeling non-covalent interactions between hydrated alkali metal cations and electrode-adsorbed OH. (b) Cation effects on surface distribution of H_{upd}, OH_{ad} and irreversible oxide. (a, b) Reproduced with permission from Ref. [50], © Macmillan Publishers Limited 2009. (c) Cyclic voltammetry of polycrystalline Pt in Ar-saturated 0.1 M MOH (M = Li: blue, Na: red, K: black). Reproduced with permission from Ref. [52], © Weber, D. J. et al. 2019. (d) pH-dependent cation effects on voltammetric peak relating to Pt (110) steps. Reproduced with permission from Ref. [53], © Wiley-VCH Verlag GmbH & Co. KGaA, Weinheim 2017. (e) Top view of TMA^+ (left top), TBA^+ (left middle) and TBP^+ (left bottom) on Pt (111). Results of natural bond orbital charge on TBA^+ and TBP^+ (right). (f) The fingerprint region of C-H peak of TBAOH and TBPOH in infrared spectra after the chronoamperometric test. (e, f) Reproduced with permission from Ref. [54], © Chung, H. T. et al. 2016. (g) Schematic illustration of cation distribution in TMA^+/TPA^+ mixtures above TMA^+ critical concentration (0.01 M). (h) Orientational distribution functions of water molecules along the surface normal in TMA^+, TEA^+, and TPA^+ electrolytes. (i) Position-resolved hydrogen-bond density profile along the surface normal. (g–i) Reproduced with permission from Ref. [55], © Zhao, K. Y. et al. Published by the Royal Society of Chemistry 2023.

molecules, thereby enhancing the kinetic rates of HOR [55]. The study found that the peak values of water molecule density and hydrogen bond number with the distance from the electrode surface correspond to the water layer extending from the electrode surface. The density of water molecules and the number of hydrogen bonds in the first layer of water significantly decrease with the increase of organic cation size, i.e., TMA > TEA > TPA, which means that larger volume organic cation TPA can more effectively displace the adsorbed water on the Pt surface (Figs. 2(g)–2(i)). At the same time, the characteristic peak intensity of water molecule density and the uniformity of hydrogen bond distribution between the second and third layers of water are positively correlated with the size change of organic cations, indicating that when larger organic cations are present, water molecules in different layers form stronger interlayer connections through hydrogen bonds. The orientation distribution of the first layer of water molecules further confirms that compared to TMA, TPA is more favorable for the formation of interlayer hydrogen bonds. For HOR, the reaction involves the shuttling of protons between the electrode-electrolyte interface and the bulk electrolyte, and the interconnection between different layers of water molecules at the interface is crucial. Therefore, larger organic cations can promote interfacial interlayer connections through hydrogen bonding, thereby enhancing proton shuttle and HOR activity.

3.1.2 *Hydrogen evolution reaction*

The hydrogen evolution reaction (HER) is pH dependent and can be categorized as acidic and alkaline HER. In acidic systems, the reactants for HER are hydrated hydrogen ions, while in alkaline systems, water molecules are often regarded as reactants. Previous studies have confirmed that alkaline HER kinetics limitations arose neither from hydrolysis dissociation/formation energy barriers nor hydrogen adsorption strength [56]. Instead, the distribution of water in the EDL and the connectivity of the hydrogen-bond network play a major role. The electrode-electrolyte interface, which governs the transfer of reactants, products, and intermediates, significantly affects OH^- transfer and water molecule polarization during HER.

Cations in electrolytes influence the electrode-electrolyte interface in three ways: specific adsorption, semi-specific adsorption, and electrostatic interaction with the electrode surface. Li et al. systematized three cation-mediated electrocatalysis modulation mechanisms: (1) site blocking via specifically adsorbed

cations; (2) electron-transfer driving force alteration through cation-induced potential redistribution; (3) cations interact with the interface electric field, the dipole moment of adsorbed intermediates, and reaction intermediates, altering the structure of interfacial water [57]. The hydration of cations buffers interface pH, significantly influencing HER activity.

Research on the effect of electrolyte cations on the HER overpotential can be traced back to 1930, when Herasymenko et al. found that adding metal salts to 0.01 M HCl increased the overpotential on mercury electrodes [58]. For example, 0.1 M LiCl and RbCl increased HER overpotential by 53 and 86 mV, respectively. In addition, the overpotential increase correlated with the valence of the cation, with Li^+, Mg^{2+}, La^{3+}, and Th^{4+} causing increases of 13, 54, 79, and 104 mV, respectively. These trends were ascribed to competitive electro-sorption of protons versus cations at the electrode interface, quantified via a competitive Langmuir isotherm formalism. The cations with higher hydration energies (e.g., Li^+) exhibited stronger non-covalent interactions with the Pt surface, affecting HER activity. The order of alkali metal cations by hydration energy was: $Li^+ > Na^+ > K^+ > Cs^+$.

Markovic et al. discovered that Li^+ formed stronger interactions with H_2O and adsorbed hydroxide (OH_{ad}) compared to K^+, enhancing HER activity of $Ni(OH)_2$/Pt catalyst. They explained that Li^+ hydration in the compact layer of EDL facilitated the formation of $Ni(OH)_2$-Li^+-OH-H complexes, reducing steric hindrance or electronic effects on the interfacial water and promoting water dissociation [59]. Similarly, Jia et al. investigated the role of OH_{ad}, water, alkali metal addition (AM^+) in the EDL, showing that AM^+ induced desorption of OH_{ad} into the bulk electrolyte, thus enhancing HER kinetics [60] (Figs. 3(a) and 3(b)). As Lewis acids, AM^+ cations had a strong bond with the Lewis hard base OH^-, but a weak bond with the nearly neutral OH_{ad}, leading to unbalanced bonding energies that promoted OH_{ad} desorption and enhanced the Volmer step of HER. But this phenomenon only existed in one direction, that was, the presence of OH_{ad}-$(H_2O)_x$-AM^+ only improved HER, and did not improve HOR. However, the hydrogen binding energy (HBE) and the potential of zero charge (pzfc) theories affected the Volmer reaction steps from both the HER and HOR directions, so these two theories cannot explain the enhanced HER activity induced by AM^+. Based on the preliminary works of Markovic and Jia et al., Duan et al. systematically studied the influence of alkali cations in HER on Pt in alkaline media [61] (Figs. 3(c)–3(e)). They found that smaller AM^+ cations (e.g., Li^+) increased OH_{ad} coverage, thereby promoting HER activity. Li^+, in particular, caused minimal disruption to OH_{ad} on the Pt surface, enabling OH_{ad} to shuttle protons within hydration shells, thereby accelerating HER kinetics in alkaline media. In HER, cations not only affect the coverage of OH_{ad}, but also affect the interfacial water structure and hydrogen bonding network. Li et al. used electrochemistry, *in-situ* core-shell nanostructure enhanced Raman spectroscopy techniques to systematically study the behavior of different cationic electrolytes at the interface of Pd surface water [62]. As the size of the cation changes, there is a significant difference in the frequency vibration of the OH stretching band under the studied potential, that is Li^+ (0.1 M) < Na^+ (0.1 M) <K^+ (0.1 M) < Ca^{2+} (0.1 M) < Sr^{2+} (0.1 M) < Na^+ (5.0 M). Due to the correlation between the Raman frequency of the OH stretching vibration band and the hydrogen bonding interaction of water molecules, the higher the Raman frequency of the OH stretching vibration band, the weaker the hydrogen bonding interaction. Therefore, for cationic electrolytes with larger radii, higher valence states, and higher concentrations, the interface water at the Pd water interface exhibits weaker hydrogen bonding interactions. According to the differences in interfacial water hydrogen bonding interactions caused by different cations, the OH stretching vibration band is decomposed into three parts: low frequency, medium frequency, and high frequency. The low-frequency and high-frequency components are respectively associated with 4-coordinated and 2-coordinated hydrogen bonded water, while the high-frequency component is associated

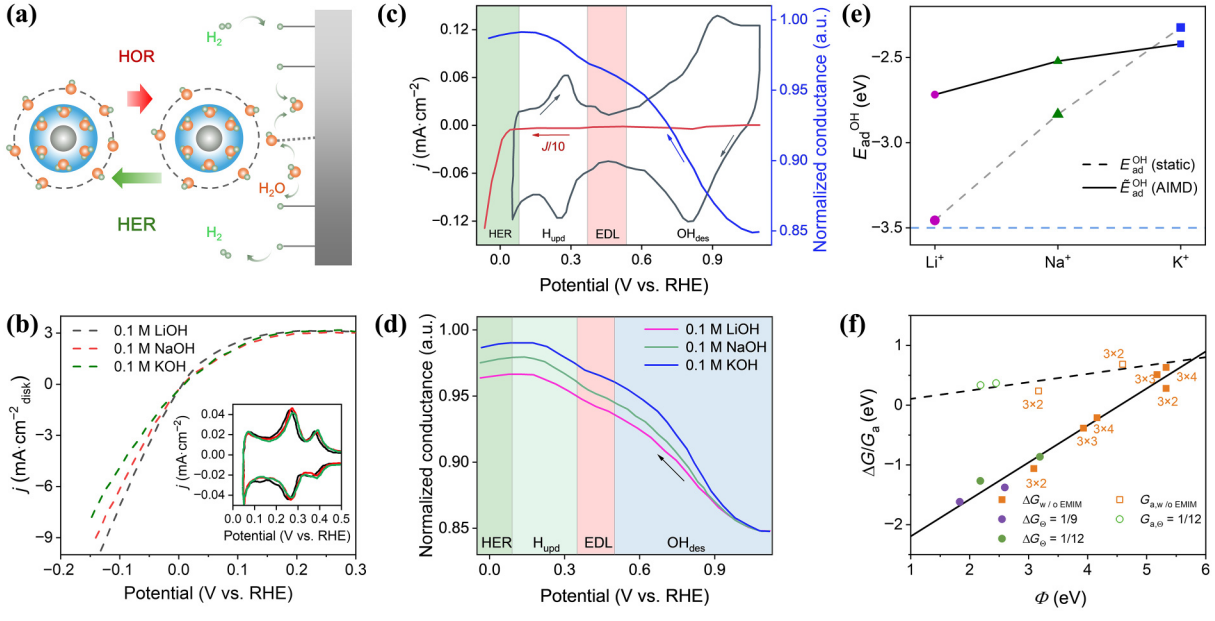

Figure 3 (a) The roles of OH_{ad}-$(H_2O)_x$-AM^+ in the alkaline HER kinetics. (b) Polarization curves of the Pt polycrystalline in 0.1 M MOH (M=Li, Na, K). The inset presents the CV curves. (a, b) Reproduced with permission from Ref. [60], © American Chemical Society 2019. (c) Typical CV (black), negative sweeping branch (red) and ETS spectrum (blue). (d) Potential-dependent normalized ETS conductance for PtNW electrode in 0.1 M MOH (M = Li, Na and K) electrolyte. (e) Cation-modulated OH adsorption energetics from static calculations and AIMD simulations. The dotted horizontal line marks the adsorption energy without cation. (c–e) Reproduced with permission from Ref. [61], © Shah, A. H. et al. under exclusive licence to Springer Nature Limited 2022. (f) Work function dependence of Volmer step energetics for bare and $[EMIM]^+$-covered Ag(111) surfaces. Reproduced with permission from Ref. [63], © American Chemical Society 2017.

with cation bound water with weak hydrogen bonding interactions. At the research potential, the proportion of cation bound water in the OH stretching vibration bands of 0.1 M Li^+, Na^+, K^+, Ca^{2+}, Sr^{2+}, and 5.0 M Na^+ electrolytes was 18.6%, 22.9%, 23.6%, 43.7%, 47.9%, and 52.1%, respectively. Density functional theory (DFT) calculations showed that the coordination numbers of water molecules around Li^+, Na^+, K^+, Ca^{2+}, and Sr^{2+} were four, five, six, six, and eight, respectively, which was consistent with the enrichment phenomenon of cation bound water in *in-situ* Raman results. In addition, water molecules with two dangling hydrogen atoms in cationic systems exhibited structural differences. With the increase of cation radius and valence state, hydrogen atoms that were originally far away from the electrode will be oriented closer to the surface, forming a structure where two of hydrogen atoms are directed toward the electrode surface, that is, a two-H down structure. This indicates that changing the cation can effectively regulate the structure of interfacial water. Cations with higher valence states and larger ionic radii can generate more water molecules with a two-H down arrangement at the Pd surface, which can effectively enhance the HER reaction rate.

In addition to alkaline cations, organic cations also influence HER activity. Jaramillo et al. explored the pH-dependent effects of 1-ethyl-3-methylimidazolium ($EMIM^+$) on the HER of Ag, Cu and Fe electrodes [63] (Fig. 3(f)). At pH=1, the presence of $EMIM^+$ significantly reduced the current density of all three catalysts, particularly Fe, where the current density dropped by 75 % at −0.5 V_{RHE}. In alkaline solutions (pH 13), the role of $EMIM^+$ on HER was negligible, likely because $EMIM^+$ competes with H_3O^+ for active sites in acidic conditions but has little effect on neutral H_2O diffusion in alkaline conditions. Further, Sequeira et al. studied the effects of specific adsorbed anions in ionic liquids on HER activity in alkaline electrolytes by using [EMIM][Ac] (acetate), [EMIM] [$EtSO_4$] (ethylsulfate), and [EMIM][$MeSO_3$] (methane sulfonate) [64]. They found that $[MeSO_3]^-$ resulted in the highest HER current, while $[Ac]^-$ and $[EtSO_4]^-$ inhibited HER. The addition of ionic liquids reduced total impedance, likely due to the pre-adsorption of the ionic liquid, which stabilized intermediate hydrogen atoms and altered charge transfer processes at the electrode-electrolyte interface.

3.1.3 *Oxygen evolution reaction*

The oxygen evolution reaction (OER) is an important semi-reaction in water electrolysis equipment, with a theoretical potential of 1.23 V_{RHE} [65]. The relentless pursuit of researchers is to achieve efficient OER processes at lower overpotentials. While a large amount of research has focused on developing efficient OER catalysts and improving stability under high current densities, the impact of electrolytes on OER activity is less understood. Recent studies have demonstrated that both electrolyte cations and anions significantly affect OER activity, including alkali metal cations and anions. A deeper understanding of these effects can provide insights into changes in the EDL during OER and inform the development of more efficient OER catalysts.

Kitchin et al. investigated the effect of different alkaline electrolytes and Fe^{3+} content on the OER performance of NiOOH catalysts [66] (Fig. 4(a)). In Fe^{3+}-free electrolytes, the OER activity followed the trend $Cs^+ > K^+ \approx Na^+ \approx Li^+$, when the overpotential was greater than 0.45 V. However, with the introduction of Fe^{3+} impurities, the OER current density in Fe^{3+}-saturated KOH and NaOH significantly increased compared to that of CsOH and LiOH. At an overpotential of 0.3 V, KOH and NaOH exhibited a current density of 7 mA·cm^{-2}, while CsOH and LiOH reached 4.5 and 2.5 mA·cm^{-2}, respectively. Compared to purified electrolytes, the introduction of Fe^{3+} reduced the overpotential of the four electrolytes by at least 100 mV. The enhanced performance in KOH and NaOH electrolytes was attributed to the interaction between Fe^{3+} and K^+, Na^+. Further, Raman spectroscopy was used to study CsOH and LiOH, showing peak shifts at 480 cm^{-1} (O-Ni-O bending) and 560 cm^{-1} (O-Ni-O stretching) under different overpotentials before and after Fe^{3+} introduction. For purified CsOH, the peak positions were 1.5−5.0 cm^{-1} lower than for LiOH, indicating that CsOH promoted the NiOOH active phase with longer Ni-O bonds, resulting in higher OER current density [67]. After Fe^{3+} was added, the Raman spectra showed only minor changes, suggesting that Fe^{3+} had little impact on the NiOOH structure.

Likewise, Koper et al. also confirmed that the OER activity followed the order $Cs^+ > Na^+ > K^+ > Li^+$ in purified 0.1 M MOH [68] (Fig. 4(b)). Although widespread recognition of cation-dependent OER kinetics, the exact mechanism remains unclear. Grimaud et al. suggested that cation-oxygen electrostatic coupling at electrified interfaces as the dominant factor to explain cation-dependent OER activity trends [69] (Figs. 4(c) and 4(d)). By studying the cyclic voltammetry of the electrodeposited NiOOH film in Fe-free 0.1 M MOH (M=Li^+, Na^+, K^+, TBA^+ and TMA^+), it was found that no change in the oxidation potential from Ni^{2+} to Ni^{3+} was observed for Li^+, Na^+ and K^+. For TBA^+ and TMA^+, a positive shift in the oxidation potential from Ni^{2+} to Ni^{3+} was observed. For Fe containing membranes, cations strongly influenced the Ni^{3+}/Ni^{2+} redox peak, with a potential difference of 78 mV between K^+ and TMA^+, indicating that Fe-free and Fe-containing membranes had different affinities for TBA^+ and TMA^+. Further research on the oxidation-reduction process from Ni^{2+} to Ni^{3+} revealed that pure NiOOH membranes had a cation independent potential-pH dependent value of −60 mV/pH. When pH > 12.5, the potential pH dependent value of the Fe-containing film was −90 mV/pH, indicating that the Fe-containing film had different deprotonation mechanisms. The OER test also showed that from Na^+, K^+ to TMA^+, the Tafel slope of the Fe-containing membrane changed from 35 to 55 mV·dec^{-1}, indicating that TMA^+ can regulate the OER mechanism based on its interaction with the membrane. Isotope testing was conducted to understand information about the OER mechanism and hydrogen bonding network. For Fe-free membranes, the OER activity in H_2O and D_2O was consistent. However, the OER activity of the Fe-containing film in D_2O was significantly reduced, accompanied by an increase in Tafel slope, indicating that the hydrogen bonding network must affect the OER kinetics by changing the number of active sites or the interaction between intermediates and adsorbed water. The introducing deuterated water would change the $*O\cdots HO^-$ interaction between active oxygen species and OH^-, thereby affecting OER activity. Diaz-Morales et al. attributed the OER performance with cation-dependence to the change in electrolyte basicity of the alkali hydroxides, which affect the adsorption energy of oxygen-containing intermediates during OER process [70] (Fig. 4(e)). Most of these studies still focus on the non-covalent interactions between electrolyte-cations and OER intermediates, while the dynamic changes in the electrocatalysts structure have not been taken into account, which may be regulated by cation insertion.

Luo et al. found that electrolyte cations could insert into the original CoOOH catalytic layer, increasing interlayer spacing and enhancing OER activity with the order $Cs^+ > K^+ > Na^+ > Li^+$ [71] (Figs. 4(f) and 4(g)). OER testing showed overpotentials of 355, 386, 399, and 406 mV at 10 mA·cm^{-2} in CsOH, KOH, NaOH, and

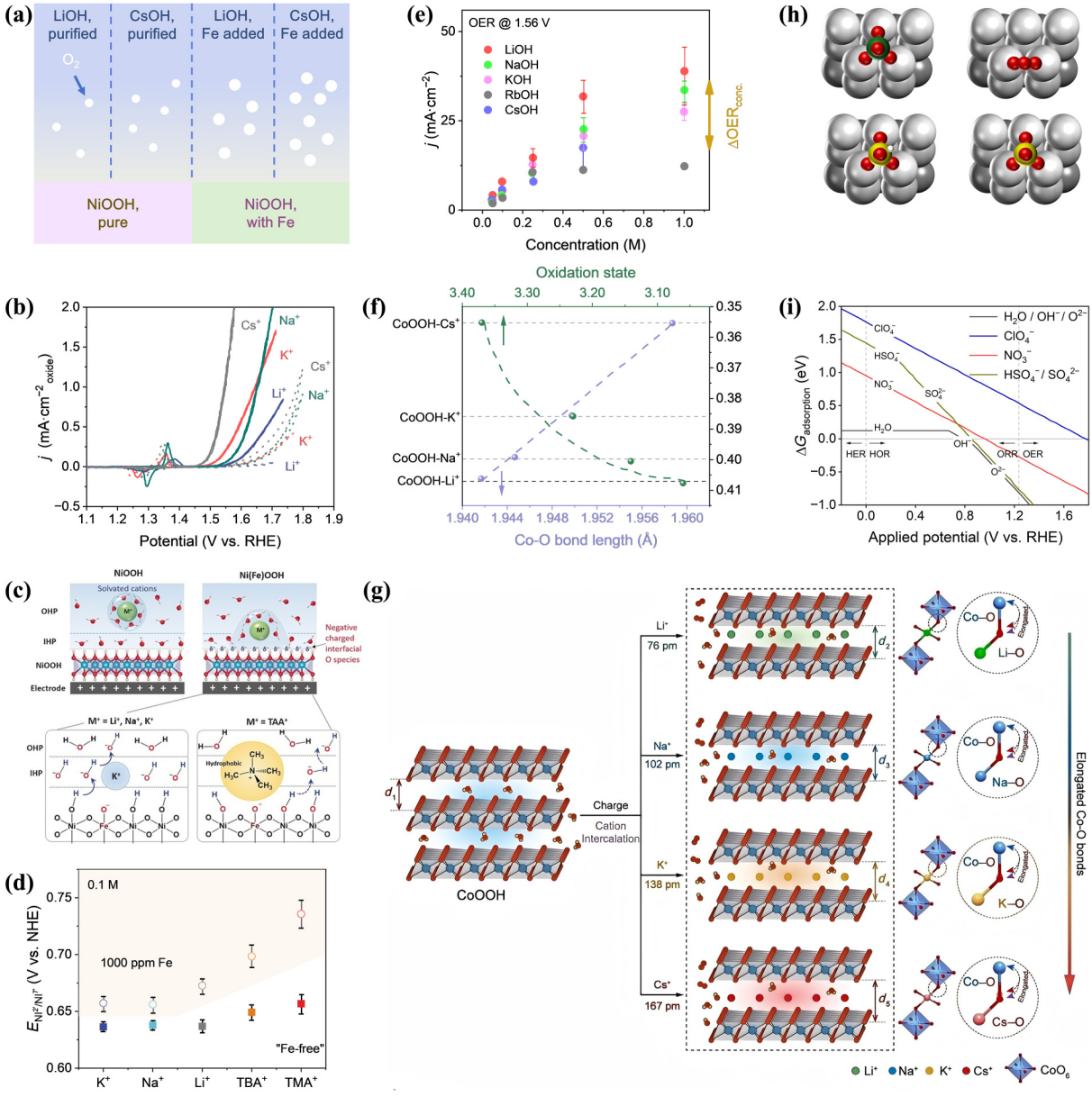

Figure 4 (a) Schematic diagram of the influence of different alkaline electrolytes and electrolyte Fe content on the catalytic activity and active structure of NiOOH. (b) CVs of NiOOH at pH 13 in various electrolytes. Reproduced with permission from Ref. [68], © Wiley-VCH Verlag GmbH & Co. KGaA, Weinheim, 2019. (c) Cation interactions with active oxygen species on pure NiOOH versus Fe-containing Ni(Fe)OOH surfaces. (d) Redox potential of $Ni(OH)_2$/NiOOH in 0.1 M MOH electrolyte. (c, d) Reproduced with permission from Ref. [69], © Yang, C. Z. et al. Published by Wiley-VCH Verlag GmbH & Co. KGaA. 2017. (e) Current density at 1.56 V vs. electrolyte concentration. Reproduced with permission from Ref. [70], © Görlin, M. et al. 2020. (f) Dependence of experimental overpotential at 10 $mA·cm^{-2}$ on Co oxidation state and Co-O bond length. (g) The schematic illustration of alkali cation intercalation and elongated Co. (f, g) Reproduced with permission from Ref. [71], © Wiley-VCH GmbH 2023. (h, i) Stable anion adsorption configurations on Pt (111) and their adsorption free energies as a function of applied potential. (h, i) Reproduced with permission from Ref. [72], © Kamat, G. A. et al. 2022.

LiOH, respectively. *In-situ* XRD revealed a negative shift in the diffraction peak of the CoOOH (003) plane as voltage increased, indicating that the insertion of cations led to an increase in interlayer spacing. At the same time, the lattice spacing of the (101) planes of CoOOH-Cs^+, CoOOH-K^+, CoOOH-Na^+ and CoOOH-Li^+ were 0.264, 0.258, 0.255 and 0.251 nm, respectively, which were greater than the original lattice spacing of CoOOH at 0.241 nm, consistent with the conclusion of *in-situ* XRD. Through the study of CoOOH-M^+ chemical bonds, it was found that cation insertion can form the Co-O-cation bridge, which can promote the kinetics of OER reaction. X-ray absorption spectroscopy further confirmed that cations with higher atomic numbers stretched Co-O bonds, optimizing the adsorption energy of oxygen-containing intermediates and enhancing OER performance. DFT calculations indicated that alkali metal cation insertion altered the d-band center of Co atoms, following the order of Li^+ (–2.18 eV) < Na^+ (–2.13 eV) < K^+ (–2.09 eV) < Cs^+ (–2.07 eV).

In addition, anions also play a significant role in OER activity. Recently, it has been found that these thermodynamically stable oxygen-containing anions can adsorb on the catalyst surface. There, they can interact with reaction intermediates, thereby altering the OER kinetics. Jaramillo et al. investigated the effects of ClO_4^-, NO_3^-, and SO_4^{2-} anions on the OER process, finding that Pt exhibited Tafel slopes of 125 and 160–170 $mV·dec^{-1}$ in $HClO_4$, HNO_3, and H_2SO_4, respectively [72] (Figs. 4(h) and 4(i)). This

indicated differences in the OER mechanism across electrolytes. The weaker adsorption of ClO_4^- resulted in higher OER activity, while stronger adsorption of NO_3^- and SO_4^{2-} led to lower activity due to competitive adsorption at active sites.

3.1.4 *Oxygen reduction reaction*

Previous research has shown that the oxygen reduction reaction (ORR) process can proceed through two primary pathways, the direct 4e⁻ reduction and series 4e⁻ reduction [73, 74]. In the direct pathway, oxygen is reduced to water in a one-step reaction in acidic media or reduced to hydroxyl ions in alkaline media. In contrast, the series pathway first reduces oxygen to a superoxide anion, which is further reduced to hydrogen peroxide intermediates in acidic media or hydrogen peroxide anion intermediates in alkaline media, before ultimately forming water or hydroxyl ions. The choice between the direct and series pathways is heavily influenced by the electrolyte, making electrolyte regulation a key strategy for controlling the thermodynamics and kinetics process of the ORR.

Zhang et al. investigated the ORR performance in NaOH and KOH solutions (0.5–14 M) and found that increasing the electrolyte concentration resulted in a monotonic negative shift in the peak potential and a significant reduction in current density, indicating inhibition of ORR activity [75] (Figs. 5(a) and 5(b)). KOH solution showed higher peak potential and current density compared to NaOH, suggesting that KOH is more favorable for ORR thermodynamics and kinetics. The ORR mechanism was found to be quasi-reversible and diffusion-controlled in both solutions, with an increase in concentration inhibiting superoxide protonation, thus shifting the process from the 2e⁻ pathway to the 1e⁻ pathway. Factors such as oxygen solubility, diffusivity, and PtOH formation were also affected, with KOH exhibiting better oxygen solubility and diffusivity, leading to enhanced ORR activity. Markovic et al. studied the influence of cations (Li^+, K^+, Ba^{2+}) on the ORR over Pt and Au surface [76] (Fig. 5(c)). On Pt electrodes, OH adsorption increased in the order $K^+ < Li^+ < Ba^{2+}$, indicating that ORR activity followed $K^+ >> Li^+ > Ba^{2+}$. Additionally, OH_{ad} stabilized by cations was observed in the hydrogen underpotential deposition (H_{upd}) region, indirectly confirming that M^{n+} may be located between the inner and outer Helmholtz layers. Surface X-ray scattering (SXS) revealed that the cations in EDL were anchored via ion-dipoleinteractions (Ba^{2+}···OH_{ad}). However, Au electrodes, the impact of cations was negligible due to the low coverage of OH_{ad}- $M^{n+}(H_2O)_x$ complexes.

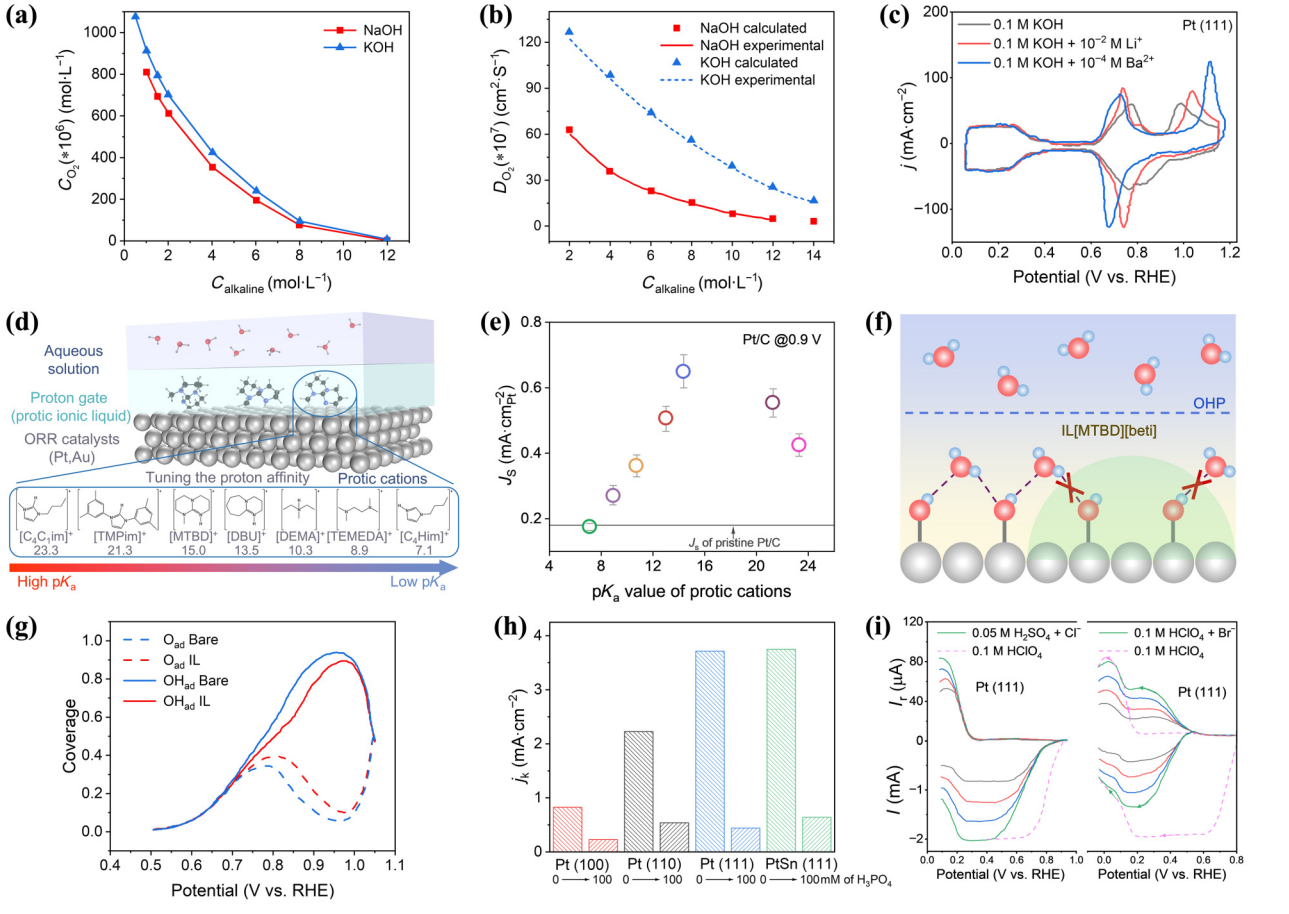

Figure 5 (a) Comparison of oxygen solubility between NaOH and KOH solutions. (b) Calculated oxygen diffusion coefficients in NaOH and KOH solutions. (a, b) Reproduced with permission from Ref. [75], © American Chemical Society 2010. (c) CVs for Pt (111) in KOH and KOH containing Li^+ and Ba^{2+}. Reproduced with permission from Ref. [76], © American Chemical Society, 2011. (d) The local proton activity is altered by adding a thin layer of protic ionic liquids (p*K*a range: 7.1–23.3) on the surface of metallic catalysts. (e) Dependence of specific ORR kinetic current on ionic-liquid-modified Pt/C on the p*K*a of protic cations. (d, e) Reproduced with permission from Ref. [77], © Wang, T. et al. under exclusive licence to Springer Nature Limited 2021. (f-g) Equilibrium coverage of adsorbed oxygenated species on Pt (111) (blue) and IL-modified Pt (111) (red) during ORR. Reproduced with permission from Ref. [78], © American Chemical Society 2022. (h) ORR kinetic current density at +0.85 V on Pt (100), Pt (110), Pt (111), and PtSn (111) single crystals in 0.1 M $HClO_4$ with/without 100 mM H_3PO_4. Reproduced with permission from Ref. [79], © the Owner Societies 2010. (i) ORR polarization curves (disk) and corresponding H_2O_2 oxidation currents (ring) on Pt (111) in different electrolytes: 0.1 M $HClO_4$, 0.05 M H_2SO_4+10^{-3} M Cl^-, and 0.1 M $HClO_4$+10^{-4} M Br^-. Reproduced with permission from Ref. [81], © Elsevier B.V. 1970.

The minimal coverage on Au reduced the effect on O_2 adsorption sites and ORR activity, in contrast to Pt, where the higher coverage enhanced ORR activity.

In addition to inorganic metal cations, organic cations in ionic liquids also play an important role in ORR. Recent studies have highlighted that the increased hydrophobicity at the Pt-ionic liquid interface and enhanced oxygen solubility contribute to improved ORR activity. Additionally, the difference in p*K*a values between ionic liquid cations and electrolyte anions also correlates with the open-circuit potential of H_2/O_2 fuel cells. Therefore, the interfacial proton activity of ionic liquids likely modifies the proton-coupled electron transfer (PCET) dynamics on metals like Pt and Au, thus affecting ORR activity. Shao-Horn et al. used ionic liquids to modify local proton activity in the interface layer between platinum and gold, investigating how different ionic liquids affect the intrinsic ORR activity [77] (Figs. 5(d) and 5(e)). They proposed that cations in ionic liquids act as interfacial proton relays, facilitating proton transfer between the bulk electrolyte and metal surface protons. Therefore, various proton cations ($[C_4C_1im]^+$ p*K*a=23.3, $[TMPim]^+$ p*K*a=21.3, $[MTBD]^+$ p*K*a=15.0, $[DBU]^+$ p*K*a=13.5, $[DEMA]^+$ p*K*a=10.3, $[TEMEDA]^+$ p*K*a=8.9, $[C_4Him]^+$ p*K*a=7.1) were used to investigate the effect of local proton activity near the active site on ORR kinetics, revealing a strong correlation between ORR activity and the p*K*a of proton cations, displaying a volcano trend. For example, ORR activity on Au/C and Pt/C increased by 5-fold and 3-fold, respectively, with the addition of ionic liquids. The highest activity was achieved when the p*K*a of the proton cation closely matched the p*K*a of the ORR product (e.g., water or hydrogen peroxide), enhancing PCET dynamics.

Further, Snyder et al. investigated the role in ionic liquids on interfacial water in the ORR process [78] (Figs. 5(f) and 5(g)). Hydrophobic ionic liquids were shown to reduce the coverage of oxidized species such as OH_{ad} at the solid-liquid interface, increasing the density of active sites. By weakening the binding of OH_{ad} through reduced solvation, the removal of OH_{ad} in the last step of the ORR mechanism was facilitated, improving turnover rates and enhancing ORR activity.

In addition to the influence of cations in the outer Helmholtz layer, specific adsorbed anions also affect ORR performance by interacting with the electrode interface.

Jaramillo et al. investigated the effects of ClO_4^-, NO_3^-, and SO_4^{2-} anions on ORR, finding that ClO_4^- exhibited the highest ORR activity, while NO_3^-, and SO_4^{2-} had significant inhibitory effects. The different adsorption strengths of these anions on the electrode surface contributed to competitive adsorption, with SO_4^{2-} showing the strongest adsorption and the lowest ORR activity. Chen et al. studied the effect of phosphate anions on the ORR performance of Pt (100), Pt (110), Pt (111), and PtSn (111) surfaces [79] (Fig. 5(h)). Firstly, based on the cyclic voltammetry, it was found that the addition of H_3PO_4 reduced the double layer current of Pt (100) and Pt (110) electrodes, and the magnitude of Pt (100) reduction was more pronounced, and the double layer current of Pt (111) increased significantly, which indicated that the adsorption of phosphate anions was more pronounced than Pt (100) and Pt (110) electrodes. Secondly, two results can be obtained by recording the ORR polarization curve. One was that the addition of H_3PO_4 caused a significant overpotential on the platinum electrode. In the presence of 100 mM H_3PO_4, the half wave potential shifts on Pt (100), Pt (110), Pt (111), and PtSn (111) were 99, 95, 141, and 102 mV, respectively, which meant that the toxic effect of phosphate adsorption on ORR decreased in the order of Pt (111) > PtSn (111) > Pt (100) > Pt (110). Another reason was that phosphate anions didn't compete with oxides during the adsorption process, as the presence of phosphate anions only caused slight hysteresis changes. As is well known, the hysteresis between the cathod and anode scan of the ORR curve was due to the formation of platinum oxide. Further research was conducted on the effect of H_3PO_4 addition on the rate determining step (RDS) of ORR process on platinum electrodes, it was found that with the increase of phosphate concentration, the transition potential between 60 and 120 mV·dec^{-1} of the four electrodes remained at 0.90 V_{RHE}, indicating that the RDS in ORR was not influenced by the adsorption of phosphate anions.

Finally, studies on the inhibitory effects of hydrochloric acid (HCl), hydrobromic acid (HBr) [80] and hydroiodic acid (HI) [81] halide anion have also demonstrated the competitive adsorption of these anions with ORR intermediates on Pt electrodes, leading to reduced ORR activity (Fig. 5(i)).

3.2 Electrocatalytic selectivity

3.2.1 CO_2 reduction reaction

The electrochemical reduction of carbon dioxide (CO_2) into economically valuable carbon-based products offers a promising strategy to mitigate the greenhouse effect, enhance CO_2 utilization, increase energy storage, and contribute to achieving carbon neutrality and peak carbon goals [82]. Significant advances have been made in CO_2 electro-reduction research, enabling highly selective conversion of CO_2 into high-value chemicals. Given the diverse range of CO_2 reduction products, such as CO, HCOOH, CH_3OH, CH_4, CH_3CH_2OH, C_2H_4, current efforts focus on identifying optimal catalytic materials and electrochemical conditions to enhance both activity and selectivity for specific products.

As an important medium for ion transport in electrochemical testing, electrolytes have a significant influence on the process of CO_2 electro-reduction. Specific and non-specific adsorption of electrolyte ions alters active site availability and intermediate adsorption / desorption behavior, ultimately modulating the activity and selectivity of CO_2 reduction. Understanding how electrolyte cations and anions affect reaction kinetics and product distribution is key to developing electrochemical systems with superior CO_2 reduction performance and high selectivity for desired products.

In 1991, Hori et al. first demonstrated that alkali metal cations in electrolytes play an important role in modulating CO_2 reduction activity and product selectivity on Cu electrodes [83] (Fig. 6(a)). They found that in the presence of Li^+, the hydrogen evolution reaction (HER) dominated over CO_2 reduction, while Na^+, K^+, and Cs^+ favored CO_2 reduction. Moreover, the selectivity towards C_2H_2, as opposed to CH_4, increased with hydrated cation size ($Li^+ < Na^+ < K^+ < Cs^+$), a phenomenon attributed to cation-induced changes in the OHP potential. Similarly, Koper et al. revealed that CO_2 electro-reduction does not proceed in the absence of alkali metal cations in a 1 mM H_2SO_4 electrolyte [84] (Fig. 6(b)). The addition of alkali cations accelerated CO formation, with a reactivity trend of $Cs^+ > K^+ > Na^+ > Li^+$, and comparable findings were observed on silver and copper electrodes. DFT calculations supported that alkali cations act as promoters for CO_2 electro-reduction by forming complexes with CO_2, facilitating the formation of CO_2^- intermediates.

Waegele, M. M. et al. further investigated selected alkali metal cation surface interactions by using tetramethylammonium

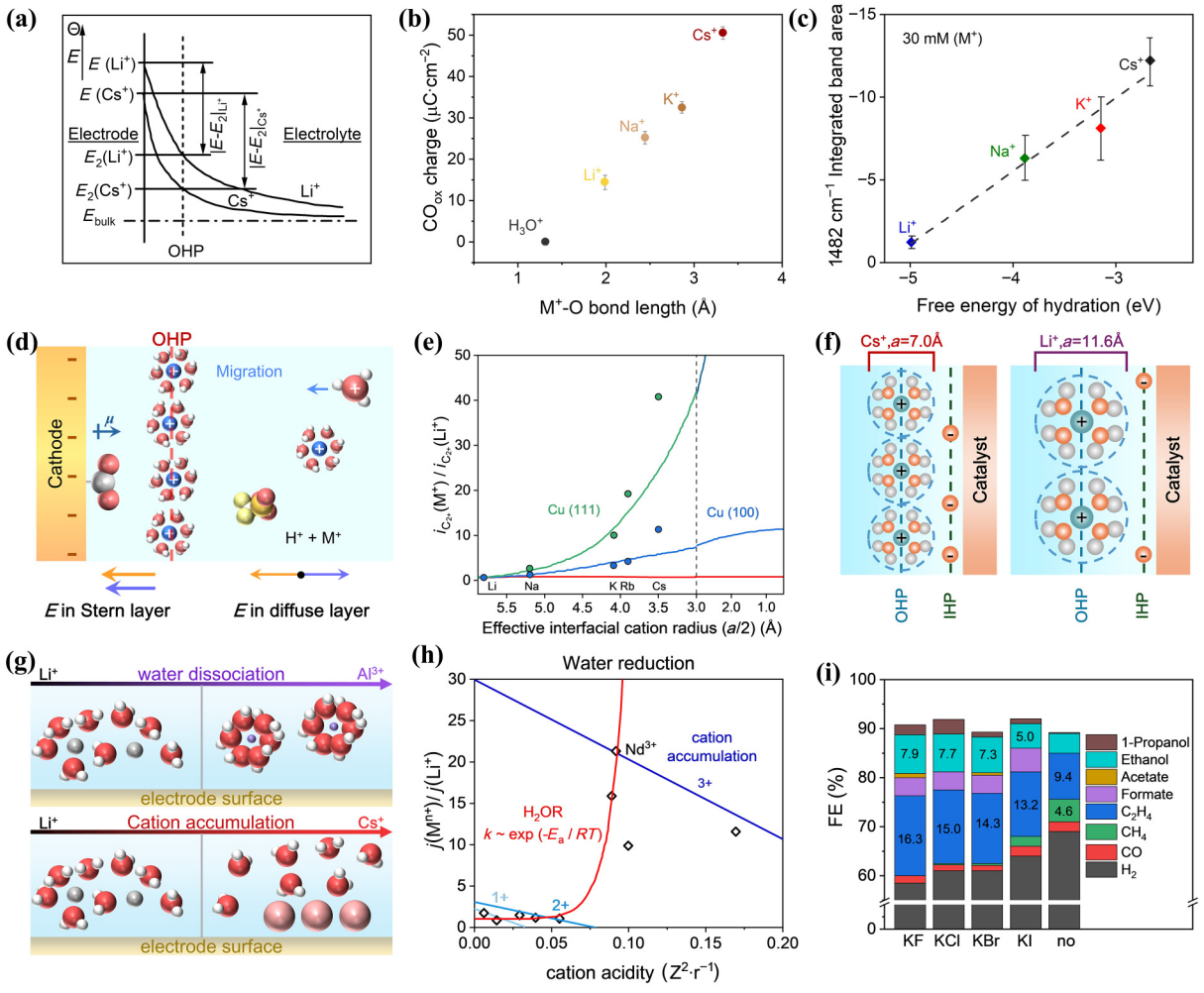

Figure 6 (a) Potential distribution in the neighborhood of the electrode. Reproduced with permission from Ref. [83], © the Chemical Society of Japan 1991. (b) CO detected on the Au electrode directly after CO_2 reduction in 1 mM M_2SO_4 with M = H, Li, Na, K or Cs. Reproduced with permission from Ref. [84], © Monteiro, M. C. O. et al. under exclusive licence to Springer Nature Limited 2021. (c) 1482 cm^{-1} band area vs. hydration free energy of alkali cations (M^+). Reproduced with permission from Ref. [85], © Ovalle, V. J. et al. under exclusive licence to Springer Nature Limited 2022. (d) Schemata of double layer near cathode in HOTf + MOTf. Reproduced with permission from Ref. [86], © Gu, J. et al. under exclusive licence to Springer Nature Limited 2022. (e) C_{2+} current density in $MHCO_3$ normalized to $LiHCO_3$. (f) Impact of hydrated cation size on catalyst surface charging. (e, f) Reproduced with permission from Ref. [87], © American Chemical Society 2022. (g) Cation-dependent water dissociation and OHP accumulation at electrode interface. (h) Normalized HER activity as a function of cation acidity (p*K*a) – Modeled coupling of H_2O dissociation kinetics and cation accumulation for mono- (1+), di- (2+), and trivalent (3+) cations. (g, h) Reproduced with permission from Ref. [88], © Monteiro, M. C. O. et al. Published by American Chemical Society 2022. (i) Product distributions as a function of halide identity (–1.0 V_{RHE}). Reproduced with permission from Ref. [92], © WILEY-VCH Verlag GmbH & Co. KGaA, Weinheim 2016.

($merthyl_4N^+$) as a vibrational probe [85] (Fig. 6(c)). By monitoring the asymmetric CH_3 deformation patterns of $merthyl_4N^+$, two subgroups were identified: hydrated $merthyl_4N^+$ and specifically adsorbed $merthyl_4N^+$. The latter subgroup was replaced by alkali metal cations under catalytic electrode potential, so it was selected as the probe. Their findings revealed that cation coverage on the electrode surface increased with decreasing hydration free energy of the cations ($Cs^+ > K^+ > Na^+ > Li^+$), and its coverage was related to the hydration free energy of alkali metal cations themselves. Additionally, Hu et al. explored the electric field induced by K^+ cations near the electrode surface, discovering that the addition of K^+ enhanced the local electric field in the Stern layer while weakening it beyond 2 nm from the cathode, ultimately inhibiting HER and promoting efficient CO_2 reduction through interactions between the electric field and dipole moments of intermediate [86] (Fig. 6(d)).

Bell et al. examined the influence of alkali metal bicarbonate ($MHCO_3$, M=Li^+, Na^+, K^+, Rb^+, and Cs^+) electrolytes on Cu electrode CO_2 electro-reduction, showing that the formation of $HCOO^-$, C_2H_4 and C_2H_5OH exhibited hydrated cation size dependent effect, following the order of $Cs^+ > Rb^+ > K^+ > Na^+ > Li^+$, while the formation of H_2, CO and CH_4 remains unaffected by cation size [87] (Figs. 6(e) and 6(f)). These trends were attributed to the variations in electrostatic field intensity in the bilayer, driven by the decrease of hydration cation radius in outer Helmholtz layer and the increase of the pzfc value of metal catalyst. The increased electrostatic field intensity contributed to the stable adsorption of intermediates with significant dipole moments, such as $*CO_2$ and *OCCO, thereby increasing the selectivity towards C_{2+} products. Dynamic control of cathode potential was identified as an effective way to regulate the distribution of CO_2 reduction products. By studying pulse electrolysis, it was found that shorter potential pulses enhanced the Faraday efficiency (FE) of C_{2+} products by allowing more frequent access to a transient enhanced state. This indicated that maintaining high local pH and CO_2 concentration were critical factors in improving the FE of C_{2+}

products. Following the study of monovalent cations, attention was directed to the influence of multivalent metal cations on CO_2 electro-reduction activity and selectivity. Koper et al. investigated the effects of multivalent cations (Li^+, Cs^+, Ca^{2+}, Ba^{2+} and Nd^{3+}, etc.) on the CO_2 electro-reduction process and competitive HER [88] (Figs. 6(g) and 6(h)). At low overpotential, the cations did not affect proton reduction but were beneficial for CO_2 electro-reduction. The activity of CO production increased in the order of $Li^+ < Na^+ < K^+ < Cs^+$. Meanwhile, it was found that electrolytes containing Cs^+ and K^+ could produce more CO at lower potentials compared to Na^+ and Li^+ which was due to the stronger coordination ability of Cs^+ and K^+ with the adsorbed CO_2^- reaction intermediates. At high overpotential, the activity of CO production followed the order of $Cs^+ > Ba^{2+} > Li^+ > Ca^{2+}$. The specific effects of these cations were found to influence water dissociation and the stability of $*CO_2^-$ intermediates, determining the competition between CO_2 electro-reduction and H_2O reduction. Further investigation revealed that the cation acidity determined the cation accumulation and hydrolysis kinetics at the OHP site. Softly hydrated cations, such as Cs^+, Ba^{2+} and Nd^{3+}, exhibited the lowest cation-cation repulsion and accumulated at the OHP site. In addition, water dissociation occurred without barriers in the presence of acidic cations, further stabilizing the coordination between cations and $*CO_2^-$ intermediates, thereby facilitating the CO_2 reduction process. Moreover, trivalent cations and weakly hydrated ions showed more continuous coordination, resulting in higher CO_2 reduction activity, following the order of $Cs^+ < Ba^{2+} < Nd^{3+}$. However, Shao-Horn et al. found that smaller and more acidic alkali metal cations can significantly enhance the conversion kinetics of CO_2 to methanol on immobilized molecular cobalt catalysts, contrary to the observed trends of CO and C_{2+} [89]. Experiments have shown that CO was the main product of CO_2RR in bicarbonate electrolytes. Notably, at potentials more positive than –0.7 V_{RHE}, CO was the primary product (up to ~90% selectivity). However, at more negative potentials, the CO output began to decrease due to its further reduction to methanol. Crucially, in this methanol-forming regime, larger cations ($Li^+ < Na^+ < K^+ < Cs^+$) resulted in higher detected CO levels, directly pointing to faster CO-to-methanol conversion kinetics with smaller cations. The kinetic isotope effect (KIE) experiment and the pH-dependent potential mismatch phenomenon on the standard hydrogen electrode (SHE) scale further confirmed the proton involvement in the reaction mechanism of methanol generation on molecular cobalt catalysts and the protonation of *CHO as the RDS of the reaction. Molecular dynamics simulations revealed that while the strongly bound hydration shell of small cations (e.g., Li^+) hinders their direct approach to the *CHO intermediate, it simultaneously enriches the interfacial water network and hydrogen bonds around *CHO. This facilitates proton transfer. Furthermore, small, acidic cations with high hydration energy polarize water molecules, promoting proton transfer to the *CHO intermediate. Consequently, smaller and more acidic cations effectively accelerate methanol generation.

In addition to cations, anions in electrolytes also play a significant role in the activity and selectivity of CO_2 electroreduction. Bell et al. investigated the effects of anions with buffering ability (HCO_3^-, HPO_4^{2-} and H_3BO_3) and without buffering ability (ClO_4^- and SO_4^{2-}) on CO_2 electro-reduction of Cu electrodes [90]. Non-buffering anions showed no impact on CO_2 electro-reduction, while buffering anions modulated the selectivity towards H_2 and CH_4, following the order of $HCO_3^- < H_3BO_3 < HPO_4^{2-}$. This phenomenon was attributed to their p*K*a values, following the order of HCO_3^- (10.33) > H_3BO_3 (9.23) > HPO_4^{2-} (7.21), consisting with H_2 formation being rate-limited by H atom generation via proton-electron transfer, while CH_4 formation is constrained by the *CO hydrogenation rate.

Strasser et al. further explored the effect of halogen anions (Cl^-, Br^- and I^-) on the CO_2 electro-reduction process. The presence of Cl^- and Br^- inhibited the HER and enhanced CO selectivity [91]. On the contrary, the addition of I^- inhibited CO production but promoted CH_4 formation. Additionally, although Br^- and I^- induced the surface morphology of Cu electrodes, the effect of halogen anions on the CO_2 reduction performance was primarily driven by their adsorption on the electrode surface. DFT calculations confirmed that halides adsorb onto the electrode surface, with the charge retention ability following the order $I^- < Br^- < Cl^-$. Therefore, the I^- on the Cu electrode surface provided more charge, promoting charge transfer to CO_2 and CO. Bell et al. further examined the effect of halide anions on surface recombination of polycrystalline Cu electrodes [92] (Fig. 6(i)). It was found that the recombination rate was highly sensitive to halogens, increasing in the order $I^- < Br^- < Cl^- < F^-$, which was consistent with the solubility of copper halides, leading to a thicker Cu_2O layer. In addition, regardless of the type of halogen anion used, the recombined Cu electrode exhibited superior HER suppression and enhanced CO_2 electrochemical activity.

3.2.2 N_2 reduction reaction

The electrochemical nitrogen reduction reaction (NRR) to synthesize ammonia offers a more sustainable and economical alternative to conventional ammonia production methods. However, the high overpotential required for NRR leads to competition with the HER, which shares similar PCET pathways. In practice, hydrogen atoms are more readily adsorbed on the electrode surface compared to nitrogen atoms, and HER exhibits faster electron transfer kinetics than NRR. Consequently, HER becomes the dominant competing reaction, consuming electrons that would otherwise contribute to NRR, thereby decreasing both ammonia yield and FE. To overcome this challenge, it is crucial to suppress HER and enhance the selectivity of NRR to improve ammonia production. In addition to designing highly active and selective catalysts for NRR, regulating electrolyte composition to suppress HER has emerged as a critical strategy for improving ammonia yield and FE. Current research demonstrates that manipulating electrolyte pH (acidic, neutral, or alkaline) and employing non-aqueous electrolytes, such as organic solvents, can effectively inhibit HER and enhance NRR performance.

Roij et al. studied the effect of H^+ concentration in acidic electrolytes on NRR selectivity [93] (Figs. 7(a) and 7(b)). For fixing N_2 saturation and varying HCl concentrations (C=10^{-3}, 10^{-2}, 10^{-1} and 100 M), they observed that the EDL region narrowed with increasing electrolyte concentration. Higher bulk H^+ concentration resulted in increased H^+ concentration near the electrode surface, simultaneously decreasing N_2 availability. At low H^+ concentrations (10^{-4} and 10^{-5} M), the NRR rate was limited by the proton transfer for nitrogen species protonation. Conversely, at high H^+ concentrations (10^{-1} and 100 M), HER inhibited the progress of the NRR process. After experimental optimization, when pH=3.5, the ammonia yield and FE of the NRR process were the highest. Feng et al. studied the NRR activity of Pd electrodes across various pH conditions [94] (Fig. 7(c)). HER tests in Ar-saturated electrolytes of 0.05 M H_2SO_4 (pH = 1.2), 0.1 M phosphate buffered saline (PBS, pH = 7.2), and 0.1 M NaOH

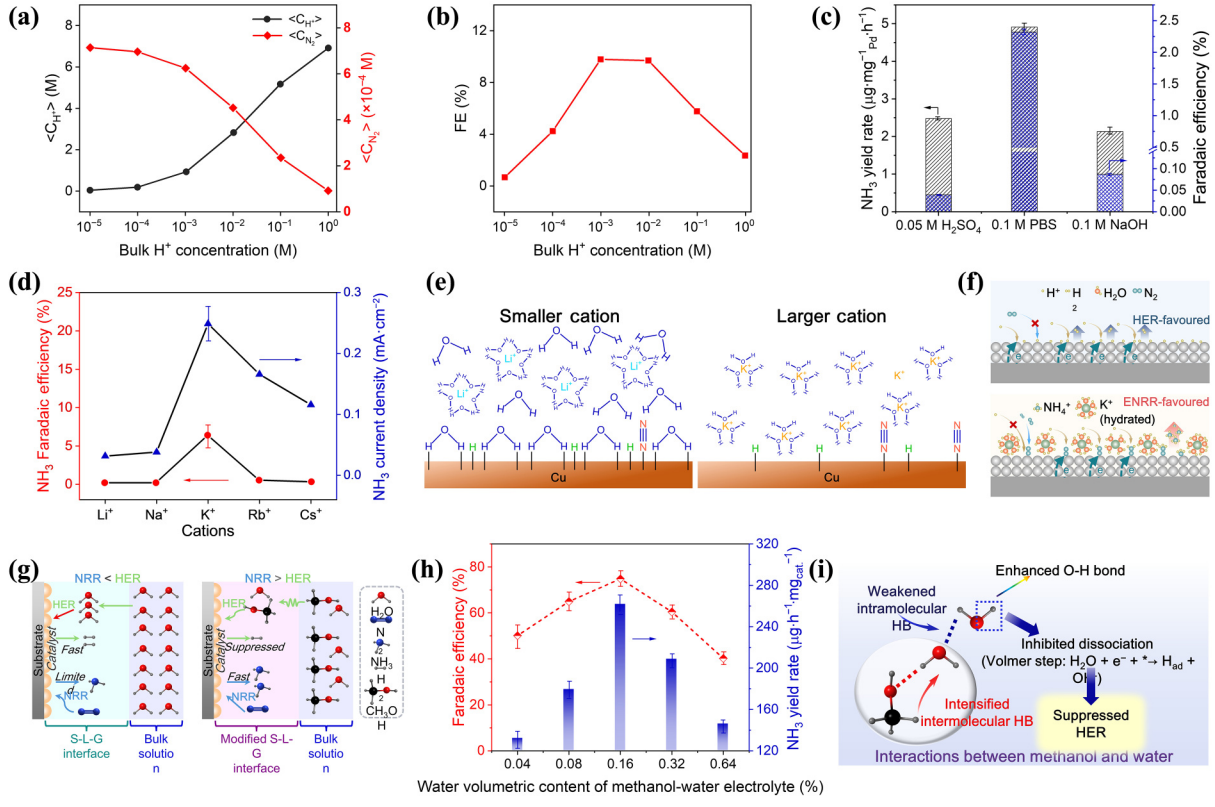

Figure 7 (a) Potential dependence of pore-averaged H^+ and N_2 concentrations at cathode surface. (b) NRR FE: Simulation vs. Experiment as a function of Ep. (a, b) Reproduced with permission from Ref. [93], © American Institute of Chemical Engineers 2021. (c) NRR performance of Pd/C: NH_3 yield rate and FE at −0.05 V_{RHE} in three N_2-saturated electrolytes. Reproduced with permission from Ref. [94], © Wang, J. et al. 2018. (d) Cation effects on NH_3 electrosynthesis: FE and partial current density. (e) Schematic representation of the effect of cations on NRR. (d, e) Reproduced with permission from Ref. [95], © American Chemical Society 2020. (f) Proton and nitrogen mass transfer in electrolytes with/without K^+. Reproduced with permission from Ref. [96], © Hao, Y. C. et al. under exclusive licence to Springer Nature Limited 2019. (g) Comparative schematics of NRR and HER reaction mechanisms at solid-liquid-gas (S-L-G) interfaces in aqueous vs. methanol-water hybrid electrolytes. (h) NRR performance metrics (FE and NH_3 yield rate) of FeOOH/CNTs at −1.2 V vs. Ag/AgCl (2 h) in methanol-water electrolytes with varied water volume fractions (0.04–0.64 vol.%). (i) Schematic depiction of methanol-water hydrogen-bonding networks and their electrostatic screening effect for HER suppression. (g–i) Reproduced with permission from Ref. [97], © American Chemical Society 2021.

(pH = 12.9) revealed that H_2SO_4 and NaOH exhibited significantly higher current densities than PBS electrolytes, indicating that neutral electrolyte effectively suppressed the HER and improved the selectivity of NRR. This suppression was attributed to higher mass and charge transfer barriers in PBS, resulting in enhanced ammonia yields at −0.05 V_{RHE}, where the FE in PBS reached 2.4% compared to less than 0.1% in both H_2SO_4 and NaOH.

Alkaline electrolytes also show promise in suppressing HER and enhancing NRR. Singh et al. explored the effects of pH and cations on NRR using Cu electrodes in alkaline conditions [95] (Figs. 7(d) and 7(e)). When the pH value was adjusted from 13 to 14, the ammonia yield and FE first increased and then decreased, and reached their maximum values at pH=13.5. As pH increased, the increase in ammonia yield and FE may be due to a decrease in NH_3 solubility and an increase in *H binding energy. Due to the close binding between NH_3 and the electrode surface, the salt precipitation effect led to a decrease in its solubility and the surface coverage of NH_3, providing more available active sites for NRR. Meanwhile, the increase in *H binding energy led to a higher *H surface coverage, resulting in a decrease in NRR active sites, which may be the reason for the decrease in ammonia yield and FE at pH > 13.5. Another reason for the decrease in FE may be that as the concentration of OH^- increased, H_2O changed from H-down to O-down at the cathode. O-down sites had a lower HER activation barrier, thereby promoting the HER process at higher pH. In addition, the role of alkali metal cations (Li^+, Na^+, K^+, Rb^+ and Cs^+) in NRR was also investigated, revealing that ammonia yield and FE increased from Li^+ to K^+, then decreased from K^+ to Cs^+. This enhancement in NRR from Li^+ to K^+ was linked to a reduction in the hydration number of larger cations, increasing the local electric field, which stabilized polar adsorbates. However, the decline in performance from K^+ to Cs^+ was attributed to the ease of water recombination in larger cation solvated shells, facilitating electron transfer to water and promoting HER over NRR. Yan et al. further demonstrated that using bismuth nanocrystals and potassium cations could enhance NRR activity and selectivity [96] (Fig. 7(f)). Increasing K^+ concentration in the electrolyte from 0.2 to 1 M resulted in a significant increase in NRR current density and FE, while HER current density decreased. DFT calculations indicated that surface-adsorbed K^+ ions reduced the ΔG for *NHH formation on Bi (012) and Bi (110) surfaces. In addition, K^+ altered the surface electronic structure of Bi, allowing more electrons to transfer to *NHH, resulting in the elongation of N-N bonds and easier activation of N_2.

In addition to aqueous electrolytes, organic electrolytes offer another route for regulating NRR performance. Qiu et al. introduced a methanol-water electrolyte system to control local proton concentration and the electrode-electrolyte microenvironment [97] (Figs. 7(g)–7(i)). The electrode-electrolyte interface of the methanol-water electrolyte system was different from the traditional solid-liquid interface. The availability of water at the

electrode-electrolyte interface can be controlled by adjusting the water content of the methanol-water system. Meanwhile, hydrogen bonding between methanol and water suppresses H_2O dissociation, thereby inhibiting HER while enhancing NRR activity. Based on FeOOH/CNTs catalysts, the methanol-water system achieved an impressive FE of 75.9% and an ammonia yield of 262.5 $\mu g \cdot mg^{-1} \cdot h^{-1}$, highlighting the potential of organic electrolytes for NRR optimization. These findings underscore the importance of electrolyte regulation, alongside catalyst design, in mitigating HER and optimizing NRR efficiency for sustainable ammonia production.

3.2.3 *Electrocatalytic conversion of small organic molecules*

With the continuous consumption of traditional fossil fuels and their serious damage to the ecological environment, biomass and its derived high value-added products have received widespread attention. The conventional process route for producing platform chemicals based on biomass usually involves extreme process conditions. For example, the conventional process of converting 5-hydroxymethylfurfural (HMF) to 2,5-furan dicarboxylic acid (FDCA) requires reaction conditions of 100 bar high pressure and 300 °C [98]. On the contrary, electrochemical catalytic technology has become a strong competitor to replace traditional production routes due to its advantages of being able to react at room temperature, atmospheric pressure, and low overpotential. Several key biomass-derived molecules, such as 5-hydroxymethylfurfural, methanol, and glycerol, have been successfully converted into valuable chemicals like 2,5-furan dicarboxylic acid, 2,5-di(hydroxymethyl)furan, and formic acid on a laboratory scale. In these transformations, product selectivity is paramount, which can not only be solved through catalyst design, but also by regulating the electrolyte composition to affect the interface microenvironment. Although significant progress has been made in developing efficient catalysts, the systematic understanding of how electrolyte components and the electrode-electrolyte interface influence product selectivity remains limited. Based on this, in this section we introduce some classic works on regulating the catalytic reaction pathway and product selectivity of organic small molecules through electrolyte anions and cations, and additives (such as ionic liquids), aiming to provide insights and guidance for the large-scale application of organic small molecule catalytic reactions.

The electrocatalytic hydrogenation (ECH) of furfural (FF) to produce furfuryl alcohol is a green and promising production route, as it proceeds without external hydrogen or high pressure. The "ionic effect" is a critical factor influencing electrocatalytic activity and selectivity, as it directly modulates the electrode-electrolyte microenvironment. Exploring the anionic effects in buffer systems such as carbonates and phosphates (which are widely used in ECH) is crucial for further elucidating the interfacial microenvironment and optimizing ECH system design. Zou et al. investigated the effect of anions on FF ECH in potassium bicarbonate and PBS [99]. It was found that the ECH current density using potassium bicarbonate electrolyte was significantly higher than that using PBS electrolyte at –0.50 V_{RHE}, with the former being 2.6 times higher than the latter. Tafel analysis revealed that without FF, the HER and ECH pathways in both electrolytes exhibited similar slopes (>120 $mV \cdot dec^{-1}$), consistent with a Heyrovsky-Volmer mechanism and comparable hydrogen surface coverage. Upon FF addition, the Tafel slope in bicarbonate decreased to ~120 $mV \cdot dec^{-1}$, markedly lower than the 160 $mV \cdot dec^{-1}$ in PBS, indicating faster hydrogenation intermediate accumulation in bicarbonate. When further using a rotating ring disk electrode to quantitatively identify the effective current of organic hydrogenation reactions, it was found that in the absence of FF, the two electrolytes exhibited similar polarization curves. However, after adding FF, the disk electrode showed stronger FF ECH kinetics in potassium bicarbonate solution. The HOR performance of the ring electrode in potassium bicarbonate was significantly weaker than PBS, which confirmed that ECH was more efficient in potassium bicarbonate and suppresses side reactions. Subsequently, the use of ED Cu electrodes for electrolysis of FF further confirmed the above conclusion. In the range of –0.3 to –0.6 V_{RHE}, the yield and Faraday efficiency of FF in potassium bicarbonate solution remained above 90%, while the optimal yield and FE in PBS were only 80% and 82% (–0.4 V_{RHE}). By calculating the hydrogen production rate and optimizing the FE composition during the electrolysis process, it was confirmed that the main charge loss was due to the occurrence of HER. This side effect was particularly significant in PBS. In addition, during the first 60 minutes of the electrolysis process, the electrolysis current in potassium bicarbonate rapidly decreased to 6 $mA \cdot cm^{-2}$, while the rate of current decrease in PBS was much slower. These results fully demonstrated the completely different hydrogenation processes in the two electrolytes. In order to gain a deeper understanding of the essence of this anionic effect, operational electrochemical impedance spectroscopy was conducted within the range of 0 to –0.6 V_{RHE}. The mid frequency region of the impedance spectrum corresponded to the Volmer step of water dissociation, which can be expressed as an intermediate accumulation process. In the ECH system, the intermediate accumulation process involves the generation of H* and the specific adsorption of organic molecules. It was found that in potassium bicarbonate solution, the Bode spectrum showed the same trend with and without the addition of FF, indicating that the organic adsorption process does not interfere with ECH. On the contrary, in the ECH system of PBS, a second characteristic peak appeared in the mid frequency region. Throughout the entire potential range, this peak exhibited significant resistance to intermediate accumulation processes, which indicated that the adsorption behavior of FF on the electrode surface was different from that of potassium bicarbonate system, and the hydrogenation process in PBS exhibited slow and unfavorable kinetic behavior. Further relaxation time distribution (DRT) analysis showed that in PBS, the adsorption process of organic molecules accounted for 50.1% of the entire intermediate accumulation process, while in potassium bicarbonate, this proportion was only 19.9%. This indicated that in the FF ECH process, most of the impedance in PBS comes from organic adsorption, while the influence of this process is relatively small in potassium bicarbonate, that is, FF exhibits weak adsorption in PBS and strong adsorption in potassium bicarbonate. Molecular dynamics simulation and radial distribution function showed that tighter molecular spacing and stronger hydrogen bonding in potassium bicarbonate electrolyte induced electrophilic activation of carbonyl groups in FF, while PBS exhibited electrophilic inhibition of carbonyl groups in FF (Fig. 8(a)). Therefore, FF ECH exhibited better kinetic characteristics in potassium bicarbonate, while it showed slow ECH kinetics and severe HER in PBS.

Traditionally, cationic effects typically exist in cathodic reactions. Cations accumulated in the inner Helmholtz layer through electrostatic interactions can generate unique electric fields and induce non covalent interactions to polarize and activate reactants and intermediates. At the anodic potential, anions

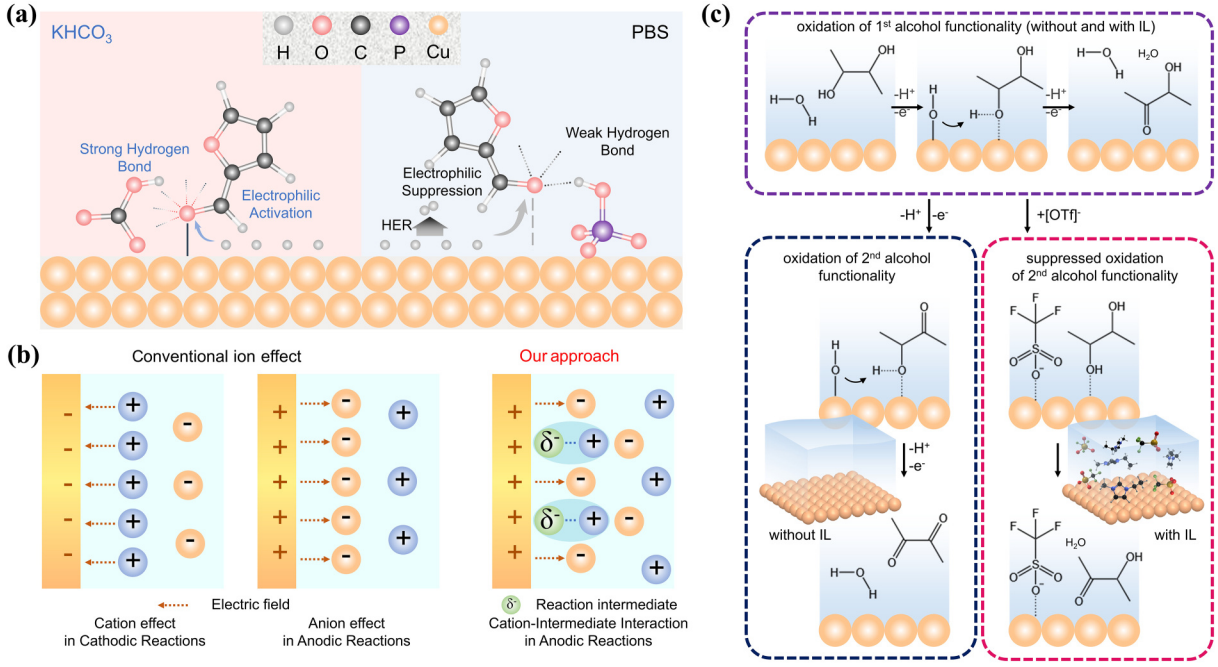

Figure 8 (a) Schematic of the anionic effect for inducing FF adsorption behaviors and carbonyl electrophilic activity change in $KHCO_3$ and PBS. Reproduced with permission from Ref. [99], © American Chemical Society 2024. (b) Scheme of the conventional ion effect and the cation intermediate interaction in the literature. Reproduced with permission from Ref. [100], © Wiley-VCH GmbH 2021. (c) Proposed mechanism for selectivity control in the electrochemical SCILL for selective oxidation. Reproduced with permission from Ref. [101], © Yang, T. *Angewandte Chemie International Edition* published by Wiley-VCH GmbH 2022.

occupy the inner Helmholtz layer, while cations typically exist in the outer Helmholtz layer. Therefore, the influence of cations on anodic reactions is usually small and rarely reported. However, Gong et al. unexpectedly found that cations selectively interact with downstream glycerol oxidation intermediates in the glycerol oxidation reaction, significantly affecting the residence time and oxidation ability of these intermediates on the electrode surface, thereby regulating the selectivity of the final product [100] (Fig. 8(b)). In the experiment, when the electrolyte changed from potassium hydroxide to lithium hydroxide, the FE of formic acid significantly increased from 64% to 81.3%. And the stability of glycerol oxidation under lithium hydroxide conditions was significantly enhanced, with only a slight decrease in FE and accumulation of 275 mM formate within 6 hours, while FE in potassium hydroxide electrolyte sharply decreased to 40%, which indicated that lithium hydroxide had a significant unconventional cationic effect on the oxidation of glycerol on $Ni(OH)_2$. From the perspective of reaction pathways, glycerol oxidation is mainly divided into two pathways: PCET (oxidation of alcohols to aldehydes or carboxylic acids) and carbon chain breakage. Only one pathway through the glyceraldehyde-glycol aldehyde intermediate can theoretically produce 100% formic acid, while other pathways can only produce 66.6% of the maximum FE. Therefore, glycerol aldehyde, acetaldehyde, glycerol acid, and ethanol acid were selected as glycerol oxidation reactants for reaction pathway analysis. The results showed that compared with lithium hydroxide, the Faraday efficiency of formic acid increased by 17% and 15.3% respectively when glycerol aldehyde and acetaldehyde were used as reactants in lithium hydroxide electrolyte, while the carboxylic acid counterparts of glycerol aldehyde and ethanol acid showed much lower cation effects, fully indicating that aldehyde intermediates may be the determining factor of selectivity. Further evidence using 1,2-propanediol as a glycerol analogue confirmed that C-C cleavage indeed occurred before aldehydes and carboxylic acids. Based on this, the author believed that in LiOH, glycerol oxidation preferentially undergoes C-C cleavage to form aldehyde intermediates and ultimately formate salts, while in KOH, it facilitates the oxidation of aldehydes to form carboxylic acids. Using the pulse amperometry method for transient dynamics research, it was found that the current decay in lithium hydroxide was significantly higher than that in potassium hydroxide, indicating a lower oxidation ability of the surface adsorption substrate in the presence of lithium cations. This delayed oxidation can create more time for nucleophilic attack of hydroxide anions to cleave C-C bonds, which in turn enhances the pathway for complete glycerol oxidation to formate. In order to elucidate the interaction between cations and intermediates, crown ethers 12-crown-4 and 18-crown-6 were selected as chelating agents for Li and K cations (represented as C-Li and C-K), respectively. It was found that the Faraday efficiency of formic acid decreased significantly under C-Li conditions, which may be attributed to fewer cation intermediate interactions and limited diffusion supply of hydroxide anions. DFT calculations indicated that the carbonyl or hydroxyl moiety is attracted to the hydrated shell of the cation through hydrogen bonding, which facilitates the adsorption of the other end on the NiOOH slab. This cation intermediate interaction also weakens the adsorption of aldehyde on the NiOOH surface, preventing subsequent oxidation.

In the electrochemical conversion reaction of small organic molecules, the yield and selectivity of the products are not only affected by the anions and cations in the electrolyte, but also by the electrolyte additive ionic liquid. Libuda et al. studied the effect of ionic liquids on the electrochemical oxidation reaction products of 2,3-butanediol, revealing the important role of ionic liquids in precise product control and selective enhancement [101]. For the electrochemical oxidation reaction of 2,3-butanediol, the main products are the singly oxidized acetoin and the doubly oxidized diacetyl. Meanwhile, hydroxyl groups must be formed on the electrode surface during the catalytic oxidation process. If the

hydroxyl groups on the electrode surface are inhibited by the ionic liquid, the reaction will also be inhibited. If there is a difference in the blocking effect of two competing reactions, the product will be altered. Based on this, the ionic liquid 1-ethyl-3-methyl-imidazolium trifluoromethanesulfonate ($[C_2C_1Im][OTf]$) was selected as an electrolyte additive. In this ionic liquid, $[OTf]^-$ not only specifically adsorbs on the Pt (111) surface, but also its coverage on the electrode surface changes with the change of potential. The experiment utilized *in-situ* electrochemical infrared reflectance absorption spectroscopy (EC-IRRAS) technology to monitor the electrocatalytic conversion process of butanediol to acetoin and diacetyl in the 0.05 to 1.1 V_{RHE} potential range. In this spectrum, the peak located at 1454–1458 cm^{-1} belongs to 2,3-butanediol and acetoin; The peaks at 1357–1362 and 1713–1715 cm^{-1} are respectively attributed to acetoin and diacetyl; The peak at 1200 cm^{-1} is a unique characteristic peak of acetoin. When no ionic liquid was added to the electrolyte and the potential exceeded 0.3 V_{RHE}, a consumption peak of 2,3-butanediol was observed at 1457 cm^{-1} in the EC-IRRAS spectrum. Simultaneously, peaks of diacetyl and acetoin formation appeared at 1713 and 1359 cm^{-1}. The most important feature was the appearance of a characteristic peak unique to acetoin at 1200 cm^{-1}. As the potential further increased, the peak intensity at 1200 cm^{-1} reached its maximum at 0.6 V_{RHE} and then decreased at higher potentials, which indicated that acetoin was initially formed with high selectivity and then further oxidized to diacetyl at potentials above 0.6 V_{RHE}. After adding the ionic liquid, the same spectral bands were observed as before, indicating that butanediol was consumed and converted into acetoin and diacetyl. However, the band intensity was completely different. Firstly, the peak intensities at 1714 and 1359 cm^{-1} representing the generation of diacetyl and acetoin significantly decreased, indicating a decrease in the catalytic activity of 2,3-butanediol reaction. At the same time, the unique characteristic peak of the Chinese zodiac appeared between 0.4 and 0.5 V_{RHE}. And when the potential exceeded 0.6 V_{RHE}, there is no sign of a decrease in peak intensity, indicating that ionic liquids can effectively block the conversion of acetoin to diacetyl, thereby significantly improving the selectivity of acetoin. In order to gain a deeper understanding of the role of ionic liquids in the catalytic reaction of 2,3-butanediol, the potential dependence of ionic liquid adsorption on the electrode surface was studied. It was found that the adsorption concentration of $[OTf]^-$ on Pt (111) surface increased with the increase of potential, while inhibiting the formation of hydroxyl groups on the electrode surface. Based on this, the regulatory mechanism of ionic liquids on the catalytic reaction products of 2,3-butanediol can be expressed as follows: the oxidation of alcohol functional groups requires co-adsorption of hydroxyl groups on the electrode surface (Fig. 8(c)). As the potential increases, the adsorbed [OTf] coating gradually increases, which not only reduces the activity of the catalytic reaction of 2,3-butanediol, but also seriously hinders the conversion of acetoin to diacetyl. However, it is accompanied by a significant increase in acetoin selectivity, which is of great significance for the large-scale preparation of intermediate products in alcohol oxidation.

4 *In-situ* characterization technology

The electrode-electrolyte interface is central to all electrochemical processes, as it governs the transport, adsorption, intermediate conversion, product formation, and desorption of reactants. During these processes, the EDL at the interface displays complex interactions, including covalent interactions between adsorbates and electrode surfaces, electrostatic interactions between electrolytes and metal surfaces, and non-covalent interactions between adsorbates and electrolytes. To advance our understanding of electrochemical reaction mechanisms, it is crucial to decipher the dynamic evolution of intermediates and the interplay of species at the electrode-electrolyte interface. A comprehensive understanding of these interactions will enable precise control of catalytic activity and selectivity in electrocatalysis.

Current research primarily focuses on the selection and optimization of electrode materials to regulate the adsorption or desorption of key intermediates in rate-determining steps of electrochemical reactions. This macroscopic approach, while effective, lacks a deep understanding of the solid-liquid interface, which is the core site of electrochemical reactions. A more nuanced understanding of the electrode-electrolyte interface could reveal strategies to regulate intermediate adsorption/desorption not only through catalyst design but also by optimizing the electrolyte. In an ideal electrochemical system, highly active and selective electrode materials, combined with electrolyte conditions that optimize the interface, would result in the most efficient and clean catalytic process.

To achieve this level of insight, advanced *in-situ* characterization techniques are essential (Fig. 9). These methods enable the construction of a dynamic and comprehensive picture of electrochemical processes, from the far-field (micrometers above the electrode surface) to the near-field (surface, subsurface, and bulk regions). Particularly important are techniques that offer high temporal and spatial resolution, which, when paired with simulations, provide a more detailed understanding of species interactions and dynamic behavior at the atomic level, guiding further optimization of electrochemical systems.

4.1 *In-situ* characterization of far-field dynamic behavior

Unlike traditional scanning probe methods, scanning electrochemical microscopy (SECM) is an established technique for quantitatively tracking the electrochemical behavior of substrates [102–105]. SECM relies on the measurement of current at the tip of an ultramicroelectrode (UME), typically on the nanometer to micrometer scale. Substrate electrochemical activity disrupts the tip's electrochemical response, providing feedback on substrate properties [106, 107]. With precise control over the probe's position in the *x*, *y*, and *z* axes, SECM allows for detailed studies of electrochemical behavior from the catalyst surface to the far-field region. SECM can also be used to image and detect chemical species at the electrode-electrolyte interface.

Common SECM modes include the generation/collection (G/C) mode, which measures current at both the tip and substrate, and the feedback mode, which collects tip current only. In G/C mode, the tip generates reactants (R) at a set potential, while the substrate is maintained at different potentials to react with and detect R. In the tip-generation/substrate-collection (TG/SC) mode, for example, the tip generates R while the substrate collects it, whereas in the substrate-generation/tip-collection (SG/TC) mode, the roles are reversed [108]. In feedback mode, the tip current is influenced by the diffusion rate of R towards the electrode. When the tip is positioned close to the substrate, the species generated at the tip can diffuse back towards the electrode and be reduced, increasing the tip current. The tip current is recorded as the tip approaches the electrode surface, providing real-time tracking of catalytic reaction kinetics at the electrode-electrolyte interface. At

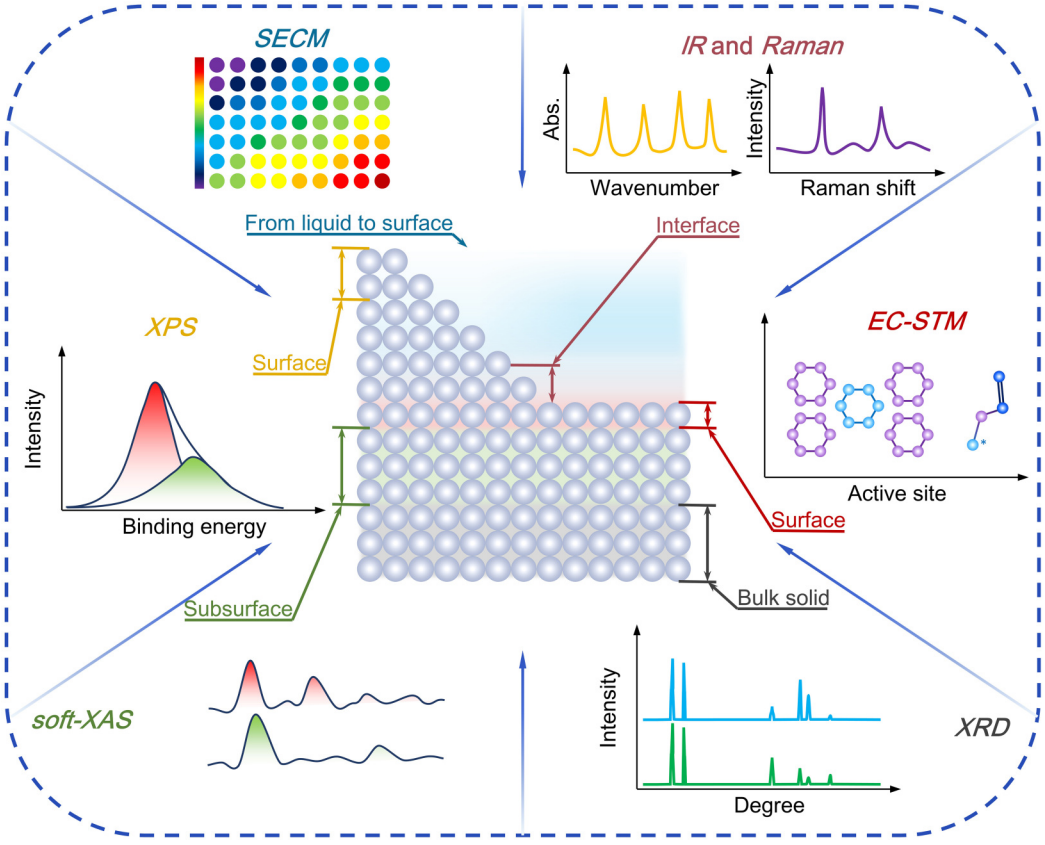

Figure 9 *In-situ* characterization technology. Dynamic solid-liquid interfaces require multimodal *in-situ* characterization spanning far-to near-field scales. Representative spectra and measurement schematics illustrate this approach.

the same time, the tip current can be recorded by scanning the tip horizontally on the substrate surface, which can obtain a chemical image of the interface morphology and reactivity. Benefiting from its high spatial resolution and diverse patterns, SECM provides convenience for *in-situ* monitoring of electrochemical reaction kinetics [109–112].

4.2 *In-situ* characterization of surface–electrolyte interactions

Surface-electrolyte interactions in electrochemical processes primarily involve the adsorption of ions and molecules, along with dipole orientation at the interface, all of which depend heavily on charge distribution within the EDL. Determining the pzfc is therefore critical. The laser-induced temperature jump (LITJ) method, which includes constant charge laser-induced potential transient (LIPT) and constant potential laser-induced current transient (LICT) modes, is commonly used to measure pzfc [113–115]. This method's advantage lies in its short time scale, and the adsorption of species (such as hydroxide groups, protons, or anions) occurs at a very slow rate compared to EDL and solvent reconstruction, so pure capacitive processes and faraday processes can be decoupled [116, 117]. Considering the correlation between pzfc and metal work function (ϕ), LITJ technology provides valuable insights into the electronic and solvent structures at the electrode-electrolyte interface as influenced by the electrolyte. Other techniques, such as ambient pressure X-ray photoelectron spectroscopy (AP-XPS) [118] and vibrational Stark spectroscopy [119], have also been employed to investigate the pzfc of electrodes. *In-situ* spectroscopic techniques, including infrared spectroscopy (IR) [120–122], Raman [123–126], and ultraviolet-visible (UV-vis) spectroscopy [127], provide molecular-level insights into the electrode-electrolyte interface. For instance, attenuated total reflection surface-enhanced infrared absorption spectroscopy (ATR-SEIRAS) offers high surface sensitivity by detecting electrolyte regions within 5–10 nm of the electrode surface. This technique is especially useful for analyzing the potential-dependent orientation of water molecules, which is sensitive to hydrogen bonding networks [128].

As a supplement to IR spectroscopy, Raman spectroscopy, particularly UV-Raman, is well-suited for studying electrochemical reactions in aqueous media due to its minimal water interference [129, 130]. In addition, due to the insufficient sensitivity of traditional Raman spectroscopy to monitor low concentration surface species at solid-liquid interfaces, surface enhanced Raman scattering (SERS) has been fully developed, where nanoscale features on metal surfaces or adsorbed organic matter can induce signal enhancement of the order of 10^6–10^9 [131]. In 2010, the shell separation nanoparticle enhanced Raman spectroscopy (SHINERS) was first reported, representing a further improvement in SERS [132]. This technology requires the synthesis of shell separated nanoparticles, and the SERS active core is covered by an ultra-thin shell, which restricts contact with the external chemical environment to prevent any direct catalytic effects of the core [133]. In recent years, the development of tip-enhanced Raman spectroscopy has also enhanced Raman intensity and spatial resolution, and adsorbates can be monitored using nano-resolution [134–137]. UV-visible spectroscopy is commonly used to determine the d-d transition of transition metal centers and charge transfer between metal-ligands [138]. Although UV visible spectroscopy technology has these characteristics, monitoring the electrode electrolyte interface remains challenging.

In addition to the above methods, mass spectrometry (MS), with its high sensitivity and exceptional selectivity, has been extensively applied for quantitative analysis in electrochemical systems [139]. Online fundamental electrochemical mass spectrometry (EC-MS) was first established in the 1970s [140]. After decades of development, EC-MS technology has been continuously updated and optimized [141, 142]. In terms of ionization of mass spectrometry, electron ionization and electric spray ionization [143–145] are commonly used methods. Other ionization technologies include thermal spraying [146], fast atomic bombardment [147], flowing atmospheric afterglow [148], and inductively coupled plasma [149]. In addition, more advanced desorption electrospray ionization mass spectrometry (DEMS) [150] and secondary ion mass spectrometry (SIMS) [151] have been fully practiced in the analysis of electrode-electrolyte interface. The combination of EC and MS can achieve real-time *in-situ* monitoring of electrocatalytic reaction species at the molecular level [152].

4.3 *In-situ* characterization of subsurface and bulk

X-ray techniques, including X-ray photoelectron spectroscopy (XPS) [153–156], X-ray absorption spectroscopy (XAS) [157–161], and X-ray diffraction (XRD), are powerful tools for probing the subsurface and bulk regions of electrode-electrolyte interfaces. XPS typically detects surface properties within a few nanometers, while XAS and XRD provide insights into deeper bulk phases. Techniques such as grazing incidence XRD and soft X-ray spectroscopy have been further developed to explore near-surface phenomena [162–165]. The advent of synchrotron radiation has led to the development of advanced techniques like X-ray emission spectroscopy (XES) [166–168], and resonant inelastic X-ray scattering (RIXS) [169–171], which offer enhanced resolution for studying electronic structures and catalytic states.

In addition to X-ray technology, *in-situ* liquid phase transmission electron microscopy (TEM) is also one of the subsurface and bulk detection techniques for electrode-electrolyte interfaces [172–175]. *In-situ* liquid phase transmission electron microscopy has an ultra-high energy electron excitation source and elastic scattering of ultrashort wavelength electron beams, so its detection depth can be from the surface to the body, and it can track the dynamic changes in the morphology and structure of catalysts during the electrocatalytic process [176, 177]. By combining electron diffraction and electron energy loss spectroscopy, *in-situ* liquid phase TEM allows for real-time tracking of dynamic changes at the electrode-electrolyte interface [178].

5 Conclusions and perspectives

In this review, we elaborate in detail on the important influence of electrolytes on the electrocatalytic reaction process from the understanding of electrode-electrolyte interface and its model development, the influence of electrolytes on the activity and selectivity of electrocatalytic reactions and the development of *in-situ* detection technology of electrode-electrolyte interface. For a long time, research on electrocatalytic processes has mainly focused on the design and development of high-performance electrode materials, while the electrolyte environment that affects the diffusion of reactant and product molecules, ion transport and the adsorption and desorption of key reaction intermediates has not been effectively studied. This review summarizes the published results on the impact of electrolytes on the performance of various electrocatalytic reactions based on previous work. Starting from the anions and cations that make up electrolytes, this review elaborates on their promoting/inhibiting effects on reaction activity and selectivity, and explores in depth the scientific theories and mechanisms behind these effects, which aims to provide reference for designing better and more matching electrolytes for various electrocatalytic reactions, and also to provide guidance for researchers who have just entered the field to quickly understand the cutting-edge dynamics and development progress of the field. Although preliminary research has been conducted on the influence of electrolytes on electrocatalytic reactions, there are still many aspects worth further investigation in the future. The specific aspects are listed below.

(I) Theoretical calculations and simulations complement experimental data by elucidating the mechanisms behind electrochemical phenomena. Despite advances in computational methods, significant gaps persist between simulated and experimental results, primarily due to over-simplified models of the electrode-electrolyte interface. This idealization distorts critical interfacial properties—especially vital in electrocatalysis—which are often overlooked. New computational strategies are urgently needed to bridge theory and reality for key interfacial characteristics like local pH, structure, electrolyte effects, mass transfer, and conductivity.

(II) Understanding the dynamic evolution of the electrode-electrolyte interface is crucial for electrolyte optimization and enhanced electrocatalytic performance, necessitating *in-situ* monitoring. Advancing the spatiotemporal resolution of characterization tools is essential for atomic/molecular-level insights into interfacial dynamics. Therefore, developing advanced *in-situ* techniques—such as ATR-FTIR, MS, Raman spectroscopy, and XPS—is imperative. These technologies enable atomic-scale observation of the EDL's distinctive characteristics and key intermediates' formation/desorption, driving breakthroughs in fundamental theory.

(III) Current studies on electrolyte effects in electrocatalysis predominantly use single-crystal electrodes rather than practical electrode materials. Significant performance differences arise due to structural disparities: Single-crystal systems exhibit ordered lattices with predictable active sites, while practical materials (e.g., supported nanoparticles) feature complex, heterogeneous active sites—including defects and functional groups—that unpredictably alter intermediate adsorption and reaction mechanisms. Furthermore, their distinct electronic structures yield divergent responses to electrolyte ions. Transitioning from model systems to representative electrode materials is thus imperative for universally applicable insights into electrolyte-catalyst interactions.

(IV) Designing efficient, stable electrolytes is critical for the long-term operation of integrated electrochemical devices. Traditional aqueous/organic electrolytes often suffer reduced conductivity and stability under demanding conditions, hindering sustainable operation and impeding commercialization. Thus, developing advanced electrolytes—such as semi-solid systems, ionic liquids, and hybrid formulations—represents a highly promising approach.

(V) Electrolyte-catalyst matching is pivotal for maximizing electrocatalytic performance. Current pairings often use conventional electrolytes that sub-optimally align with electrode materials, limiting catalytic efficiency. Thus, a holistic approach integrating electrolytes, catalysts, and operating conditions is essential. Future efforts must target tailored electrolyte

design—optimized for specific catalysts and extreme environments (e.g., high temperature, pressure, and acidity)—to unlock peak system performance.

(VI) Integrating electrolyte effects with ionomer development is critical for advancing electrochemical devices. Current research focuses on electrolyte interactions in three-electrode systems, neglecting device-level impacts. As ionomers enable catalyst integration into functional devices, embedding performance-enhancing electrolyte ions (cations/anions) within ionomer structures offers a viable path to bridge this gap. Future work should thus prioritize designing next-generation ionomers that leverage electrolyte synergies to boost device performance.

(VII) Beyond electrolyte effects on activity/selectivity, their impact on reaction stability remains unclear, largely due to challenges in long-term *in-situ* monitoring of electrode-electrolyte interfaces. Future research must prioritize decoupling degradation mechanisms—especially under high current density—to determine whether activity loss stems from material evolution or electrolyte breakdown. Resolving this will clarify primary degradation drivers and enable targeted stability optimization.

Acknowledgements

This work was financially supported by the National Natural Science Foundation of China (52372074 and 52172179), the National Key Research and Development Program of China (2024YFE0211400), the Fundamental Research Funds for the Central Universities (JD2536, buctrc202118 and buctrc202323), the Interdisciplinary Research Center of Beijing University of Chemical Technology (Funding No. XK2023-08), the Beijing-Tianjin-Hebei Basic Research Cooperation Special Project (B2024209048).

Declaration of conflicting interests

The authors declare no conflicting interests regarding the content of this article.

Data availability

All data needed to support the conclusions in the paper are presented in the manuscript. Additional data related to this paper may be requested from the corresponding author upon request.

References

[1] Zhang, G.; Schreier, M. Leveraging electrochemical double layer structure to rationally control electrolysis. *Natl. Sci. Rev.* **2024**, *11*, nwae299.

[2] Schott, C. M.; Schneider, P. M.; Song, K. T.; Yu, H. T.; Götz, R.; Haimerl, F.; Gubanova, E.; Zhou, J.; Schmidt, T. O.; Zhang, Q. W. et al. How to assess and predict electrical double layer properties. Implications for electrocatalysis. *Chem. Rev.* **2024**, *124*, 12391–12462.

[3] Deng, B. W.; Huang, M.; Zhao, X. L.; Mou, S. Y.; Dong, F. Interfacial electrolyte effects on electrocatalytic CO_2 reduction. *ACS Catal.* **2022**, *12*, 331–362.

[4] Jiang, Y.; Huang, J. B.; Mao, B. G.; An, T. Y.; Wang, J.; Cao, M. H. Inside solid-liquid interfaces: Understanding the influence of the electrical double layer on alkaline hydrogen evolution reaction. *Appl. Catal. B: Environ.* **2021**, *293*, 120220.

[5] Zhao, H. Y.; Lv, X. M.; Wang, Y. G. Realistic modeling of the electrocatalytic process at complex solid-liquid interface. *Adv. Sci.* **2023**, *10*, 2303677.

[6] Chen, C. J.; Jin, H. Y.; Wang, P. T.; Sun, X. G.; Jaroniec, M.; Zheng, Y.; Qiao, S. Z. Local reaction environment in electrocatalysis. *Chem. Soc. Rev.* **2024**, *53*, 2022–2055.

[7] Stamenkovic, V. R.; Strmcnik, D.; Lopes, P. P.; Markovic, N. M. Energy and fuels from electrochemical interfaces. *Nat. Mater.* **2017**, *16*, 57–69.

[8] Li, C. Y.; Le, J. B.; Wang, Y. H.; Chen, S.; Yang, Z. L.; Li, J. F.; Cheng, J.; Tian, Z. Q. *In situ* probing electrified interfacial water structures at atomically flat surfaces. *Nat. Mater.* **2019**, *18*, 697–701.

[9] Wang, X.; Song, Z. F.; Liu, R. Q.; Yu, R. B.; Wang, J. Y. Recent progress in host and electrolyte engineering towards Li_2S cathode for lithium-sulfur battery. *Nano Res. Energy*, in press, DOI: 10.26599/NRE.2025.9120194.

[10] Zhang, Q. B.; Song, Z. G.; Sun, X. H.; Liu, Y.; Wan, J. W.; Betzler, S. B.; Zheng, Q.; Shangguan, J. Y.; Bustillo, K. C.; Ercius, P. et al. Atomic dynamics of electrified solid-liquid interfaces in liquid-cell TEM. *Nature* **2024**, *630*, 643–647.

[11] Zhang, S. C.; Jin, L. R.; Lu, Y.; Zhang, L. H.; Yang, J. Q.; Zhao, Q. C.; Sun, D. W.; Thompson, J. J. P.; Yuan, B.; Ma, K. et al. Moiré superlattices in twisted two-dimensional halide perovskites. *Nat. Mater.* **2024**, *23*, 1222–1229.

[12] Tang, Z.; Yang, D.; Guo, H. Y.; Lin, S. Q.; Wang, Z. L. Spontaneous wetting induced by contact-electrification at liquid-solid interface. *Adv. Mater.* **2024**, *36*, 2400451.

[13] Li, Z. B.; Liu, Q.; Li, Q.; Dong, M. D. The role of hydrated anions in hydration lubrication. *Nano Res.* **2023**, *16*, 1096–1100.

[14] Deißenbeck, F.; Surendralal, S.; Todorova, M.; Wippermann, S.; Neugebauer, J. Revealing the reaction pathway of anodic hydrogen evolution at magnesium surfaces in aqueous electrolytes. *J. Am. Chem. Soc.* **2024**, *146*, 30314–30319.

[15] Su, H.; Zhou, W. L.; Zhang, H.; Zhou, W.; Zhao, X.; Li, Y. L.; Liu, M. H.; Cheng, W. R.; Liu, Q. H. Dynamic evolution of solid-liquid electrochemical interfaces over single-atom active sites. *J. Am. Chem. Soc.* **2020**, *142*, 12306–12313.

[16] Li, H.; Xu, Z.; Li, J. C.; Siria, A.; Ma, M. Evolution of interfacial hydration structure induced by ion condensation and correlation effects. *Angew. Chem. Int. Ed.* **2025**, *64*, e202418029.

[17] Hao, B. J.; Zhou, J. Q.; Yang, H.; Zhu, C. H.; Wang, Z. K.; Liu, J.; Yan, C. L.; Qian, T. Concentration polarization induced phase rigidification in ultralow salt colloid chemistry to stabilize cryogenic Zn batteries. *Nat. Commun.* **2024**, *15*, 9465.

[18] Wang, W. J.; Yu, S.; Huang, S.; Bi, S.; Han, H. Y.; Zhang, J. R.; Lu, Y.; Zhu, J. J. Bioapplications of DNA nanotechnology at the solid-liquid interface. *Chem. Soc. Rev.* **2019**, *48*, 4892–4920.

[19] Li, M.; Mao, A. R.; Guan, Q. W.; Saiz, E. Nature-inspired adhesive systems. *Chem. Soc. Rev.* **2024**, *53*, 8240–8305.

[20] Ge, W. X.; Chen, Y. X.; Fan, Y.; Zhu, Y. H.; Liu, H. L.; Song, L.; Liu, Z.; Lian, C.; Jiang, H. L.; Li, C. Z. Dynamically formed surfactant assembly at the electrified electrode-electrolyte interface boosting CO_2 electroreduction. *J. Am. Chem. Soc.* **2022**, *144*, 6613–6622.

[21] Xu, Y.; Ma, Y. B.; Gu, F.; Yang, S. S.; Tian, C. S. Structure evolution at the gate-tunable suspended graphene-water interface. *Nature* **2023**, *621*, 506–510.

[22] Aikens, D. A. Electrochemical methods, fundamentals and applications. *J. Chem. Educ.* **1983**, *60*, A25.

[23] Xu, W. W.; Lu, Z. Y.; Sun, X. M.; Jiang, L.; Duan, X. Superwetting electrodes for gas-involving electrocatalysis. *Acc. Chem. Res.* **2018**, *51*, 1590–1598.

[24] Sebastián-Pascual, P.; Shao-Horn, Y.; Escudero-Escribano, M. Toward understanding the role of the electric double layer structure and electrolyte effects on well-defined interfaces for electrocatalysis. *Curr. Opin. Electrochem.* **2022**, *32*, 100918.

[25] Li, P.; Jiao, Y. Z.; Huang, J.; Chen, S. L. Electric double layer effects in electrocatalysis: Insights from *ab initio* simulation and hierarchical continuum modeling. *JACS Au* **2023**, *3*, 2640–2659.

[26] Yang, P. P.; Zhang, X. L.; Liu, P.; Kelly, D. J.; Niu, Z. Z.; Kong, Y.; Shi, L.; Zheng, Y. R.; Fan, M. H.; Wang, H. J. et al. Highly

enhanced chloride adsorption mediates efficient neutral CO_2 electroreduction over a dual-phase copper catalyst. *J. Am. Chem. Soc.* **2023**, *145*, 8714–8725.
[27] Shi, Y. M.; Du, W.; Zhou, W.; Wang, C. H.; Lu, S. S.; Lu, S. Y.; Zhang, B. Unveiling the promotion of surface-adsorbed chalcogenate on the electrocatalytic oxygen evolution reaction. *Angew. Chem. Int. Ed.* **2020**, *59*, 22470–22474.
[28] Xu, Y. F.; Xia, Z. M.; Gao, W. Q.; Xiao, H.; Xu, B. J. Cation effect on the elementary steps of the electrochemical CO reduction reaction on Cu. *Nat. Catal.* **2024**, *7*, 1120–1129.
[29] Cui, H.; Song, Y. Z.; Ren, D. S.; Wang, L.; He, X. M. Electrocapillary boosting electrode wetting for high-energy lithium-ion batteries. *Joule* **2024**, *8*, 29–44.
[30] Tang, B.; Fang, Y. G.; Zhu, S.; Bai, Q.; Li, X. J.; Wei, L. Y.; Li, Z. Y.; Zhu, C. Q. Tuning hydrogen bond network connectivity in the electric double layer with cations. *Chem. Sci.* **2024**, *15*, 7111–7120.
[31] Ren, W. H.; Xu, A. N.; Chan, K. R.; Hu, X. L. A cation concentration gradient approach to tune the selectivity and activity of CO_2 electroreduction. *Angew. Chem. Int. Ed.* **2022**, *61*, e202214173.
[32] Gu, Y. H.; Zhang, Y. X.; Song, X. Y.; Wang, Y. N.; Bao, A.; Zhang, D. S.; Lv, J. Y.; Zheng, Z.; Zhang, X. Y.; Liu, Z. L. et al. Fluorine-induced surface protection strategy for bifunctional high entropy electrocatalysts enables stable seawater splitting. *Nano Res. Energy* **2025**, *4*, e9120189.
[33] Zhang, Z. M.; Wang, T.; Cai, Y. C.; Li, X. Y.; Ye, J. Y.; Zhou, Y.; Tian, N.; Zhou, Z. Y.; Sun, S. G. Probing electrolyte effects on cation-enhanced CO_2 reduction on copper in acidic media. *Nat. Catal.* **2024**, *7*, 807–817.
[34] Liang, C. W.; Katayama, Y.; Tao, Y. M.; Morinaga, A.; Moss, B.; Celorrio, V.; Ryan, M.; Stephens, I. E. L.; Durrant, J. R.; Rao, R. R. Role of electrolyte pH on water oxidation for iridium oxides. *J. Am. Chem. Soc.* **2024**, *146*, 8928–8938.
[35] Shan, Y.; Zhao, X.; Fonseca Guzman, M.; Jana, A.; Chen, S. P.; Yu, S.; Ng, K. C.; Roh, I.; Chen, H.; Altoe, V. et al. Nanometre-resolved observation of electrochemical microenvironment formation at the nanoparticle-ligand interface. *Nat. Catal.* **2024**, *7*, 422–431.
[36] Zhu, S. Q.; Qin, X. P.; Xiao, F.; Yang, S. L.; Xu, Y.; Tan, Z.; Li, J. D.; Yan, J. W.; Chen, Q.; Chen, M. S. et al. The role of ruthenium in improving the kinetics of hydrogen oxidation and evolution reactions of platinum. *Nat. Catal.* **2021**, *4*, 711–718.
[37] Luo, M. C.; Koper, M. T. M. A kinetic descriptor for the electrolyte effect on the oxygen reduction kinetics on Pt (111). *Nat. Catal.* **2022**, *5*, 615–623.
[38] Yang, J. H.; Jiao, J. P.; Liu, S. Q.; Yin, Y. Y.; Cheng, Y. Y.; Wang, Y. Y.; Zhou, M.; Zhao, W. L.; Tong, X.; Jing, L. H. et al. Switching reaction pathways of CO_2 electroreduction by modulating cations in the electrochemical double layer. *Angew. Chem. Int. Ed.* **2024**, *63*, e202410145.
[39] Ge, A. M.; Videla, P. E.; Lee, G. L.; Rudshteyn, B.; Song, J.; Kubiak, C. P.; Batista, V. S.; Lian, T. Q. Interfacial structure and electric field probed by *in situ* electrochemical vibrational stark effect spectroscopy and computational modeling. *J. Phys. Chem. C.* **2017**, *121*, 18674–18682.
[40] Kang, J. W.; Shangguan, H. L.; Deng, C. Y.; Hu, Y. Y.; Yi, J. H.; Wang, X.; Zhang, X. C.; Huang, T. Additive manufacturing-driven mold design for castings. *Addit. Manuf.* **2018**, *22*, 472–478.
[41] Helmholtz, H. Ueber einige gesetze der vertheilung elektrischer ströme in körperlichen leitern mit anwendung auf die thierisch-elektrischen versuche. *Ann. Phys.* **1853**, *165*, 211–233.
[42] Helmholtz, H. Studien über electrische grenzschichten. *Ann. Phys.* **1879**, *243*, 337–382.
[43] Grahame, D. C. The electrical double layer and the theory of electrocapillarity. *Chem. Rev.* **1947**, *41*, 441–501.
[44] Gouy, M. Sur la constitution de la charge électrique à la surface d'un électrolyte. *J. Phys. Theor. Appl.* **1910**, *9*, 457–468.
[45] Chapman, D. L. A contribution to the theory of electrocapillarity. *London, Edinburgh, Dublin Philos. Mag. J. Sci.* **1913**, *25*, 475–481.
[46] Debye, P.; Hückel, E. The theory of electrolytes. I. Freezing point depression and related phenomenon. *Phys. Z.* **2019**, *24*, 185–206.
[47] Stern, H. O. Zur theorie der elektrolytischen doppelschicht. *Z. Elektrochem. Angew. Phys. Chem.* **1924**, *30*, 508–516.
[48] Conway, B. E.; Bockris, J. Q.; Ammar, I. A. The dielectric constant of the solution in the diffuse and Helmholtz double layers at a charged interface in aqueous solution. *Trans. Faraday Soc.* **1951**, *47*, 756–766.
[49] Bockris, J. O.; Devanathan, M. A. V.; Müller, K. On the structure of charged interfaces. In *Electrochemistry*. Friend, J. A.; Gutmann, F., Eds.; Pergamon Press: New York, 1965; pp 832–863.
[50] Strmcnik, D.; Kodama, K. ; van der Vliet, D.; Greeley, J.; Stamenkovic, V. R.; Marković, N. M. The role of non-covalent interactions in electrocatalytic fuel-cell reactions on platinum. *Nat. Chem.* **2009**, *1*, 466–472.
[51] Huang, B. T.; Rao, R. R.; You, S. F.; Hpone Myint, K.; Song, Y. Z.; Wang, Y. M.; Ding, W. D.; Giordano, L.; Zhang, Y. R.; Wang, T. et al. Cation- and pH-dependent hydrogen evolution and oxidation reaction kinetics. *JACS Au* **2021**, *1*, 1674–1687.
[52] Weber, D. J.; Janssen, M.; Oezaslan, M. Effect of monovalent cations on the HOR/HER activity for Pt in alkaline environment. *J. Electrochem. Soc.* **2019**, *166*, F66–F73.
[53] Chen, X. T.; McCrum, I. T.; Schwarz, K. A.; Janik, M. J.; Koper, M. T. M. Co-adsorption of cations as the cause of the apparent pH dependence of hydrogen adsorption on a stepped platinum single-crystal electrode. *Angew. Chem. Int. Ed.* **2017**, *56*, 15025–15029.
[54] Chung, H. T.; Choe, Y. K.; Martinez, U.; Dumont, J. H.; Mohanty, A.; Bae, C.; Matanovic, I.; Kim, Y. S. Effect of organic cations on hydrogen oxidation reaction of carbon supported platinum. *J. Electrochem. Soc.* **2016**, *163*, F1503–F1509.
[55] Zhao, K. Y.; Yu, H.; Xiong, H. C.; Lu, Q.; Gao, Y. Q.; Xu, B. J. Action at a distance: Organic cation induced long range organization of interfacial water enhances hydrogen evolution and oxidation kinetics. *Chem. Sci.* **2023**, *14*, 11076–11087.
[56] Gou, W. K.; Sun, H. M.; Cheng, F. Y. Dual active sites engineering of electrocatalysts for alkaline hydrogen evolution. *Nano Res. Energy* **2024**, *3*, e9120121.
[57] Waegele, M. M.; Gunathunge, C. M.; Li, J. Y.; Li, X. How cations affect the electric double layer and the rates and selectivity of electrocatalytic processes. *J. Chem. Phys.* **2019**, *151*, 160902.
[58] Herasymenko, P.; Šlendyk, I. Wasserstoffüberspannung und adsorption der ionen. *Z. Phys. Chem. A* **1930**, *149*, 123–139.
[59] Subbaraman, R.; Tripkovic, D.; Strmcnik, D.; Chang, K. C.; Uchimura, M.; Paulikas, A. P.; Stamenkovic, V.; Markovic, N. M. Enhancing hydrogen evolution activity in water splitting by tailoring Li^+-Ni $(OH)_2$-Pt interfaces. *Science* **2011**, *334*, 1256–1260.
[60] Liu, E. S.; Li, J. K.; Jiao, L.; Doan, H. T. T.; Liu, Z. Y.; Zhao, Z. P.; Huang, Y.; Abraham, K. M.; Mukerjee, S.; Jia, Q. Y. Unifying the hydrogen evolution and oxidation reactions kinetics in base by identifying the catalytic roles of hydroxyl-water-cation adducts. *J. Am. Chem. Soc.* **2019**, *141*, 3232–3239.
[61] Shah, A. H.; Zhang, Z. S.; Huang, Z. H.; Wang, S. B.; Zhong, G. Y.; Wan, C. Z.; Alexandrova, A. N.; Huang, Y.; Duan, X. F. The role of alkali metal cations and platinum-surface hydroxyl in the alkaline hydrogen evolution reaction. *Nat. Catal.* **2022**, *5*, 923–933.
[62] You, X. Q.; Zhang, D. A.; Zhang, X. G.; Li, X. Y.; Tian, J. H.; Wang, Y. H.; Li, J. F. Exploring the cation regulation mechanism for interfacial water involved in the hydrogen evolution reaction by *in situ* Raman spectroscopy. *Nano-Micro Lett.* **2024**, *16*, 53.
[63] Feaster, J. T.; Jongerius, A. L.; Liu, X. Y.; Urushihara, M.; Nitopi, S. A.; Hahn, C.; Chan, K.; Nørskov, J. K.; Jaramillo, T. F. Understanding the influence of [EMIM]Cl on the suppression of the hydrogen evolution reaction on transition metal electrodes. *Langmuir* **2017**, *33*, 9464–9471.
[64] Amaral, L.; Cardoso, D. S. P.; Šljukić, B.; Santos, D. M. F.; Sequeira, C. A. C. Room temperature ionic liquids as electrolyte

additives for the HER in alkaline media. *J. Electrochem. Soc.* **2017**, *164*, F427–F432.

[65] Jia, R. L.; Tan, Y.; Li, A. S.; Wang, Y. J.; Cheng, C. W. 3D ordered RuO_2/WO_3 heterostructure inverse opal arrays for highly-active and stable acidic oxygen evolution reaction. *Nano Res. Energy* **2025**, *4*, e9120141.

[66] Michael, J. D.; Demeter, E. L.; Illes, S. M.; Fan, Q. Q.; Boes, J. R.; Kitchin, J. R. Alkaline electrolyte and Fe impurity effects on the performance and active-phase structure of NiOOH thin films for OER catalysis applications. *J. Phys. Chem. C* **2015**, *119*, 11475–11481.

[67] Hardcastle, F. D.; Wachs, I. E. Determination of molybdenum-oxygen bond distances and bond orders by Raman spectroscopy. *J. Raman Spectrosc.* **1990**, *21*, 683–691.

[68] Garcia, A. C.; Touzalin, T.; Nieuwland, C.; Perini, N.; Koper, M. T. M. Enhancement of oxygen evolution activity of nickel oxyhydroxide by electrolyte alkali cations. *Angew. Chem. Int. Ed.* **2019**, *58*, 12999–13003.

[69] Yang, C. Z.; Fontaine, O.; Tarascon, J. M.; Grimaud, A. Chemical recognition of active oxygen species on the surface of oxygen evolution reaction electrocatalysts. *Angew. Chem. Int. Ed.* **2017**, *56*, 8652–8656.

[70] Görlin, M.; Halldin Stenlid, J.; Koroidov, S.; Wang, H. Y.; Börner, M.; Shipilin, M.; Kalinko, A.; Murzin, V.; Safonova, O. V.; Nachtegaal, M. et al. Key activity descriptors of nickel-iron oxygen evolution electrocatalysts in the presence of alkali metal cations. *Nat. Commun.* **2020**, *11*, 6181.

[71] Jia, H. N.; Yao, N.; Yu, C.; Cong, H. J.; Luo, W. Unveiling the electrolyte cations dependent kinetics on CoOOH-catalyzed oxygen evolution reaction. *Angew. Chem. Int. Ed.* **2023**, *62*, e202313886.

[72] Kamat, G. A.; Zamora Zeledón, J. A.; Gunasooriya, G. T. K. K.; Dull, S. M.; Perryman, J. T.; Nørskov, J. K.; Stevens, M. B.; Jaramillo, T. F. Acid anion electrolyte effects on platinum for oxygen and hydrogen electrocatalysis. *Commun. Chem.* **2022**, *5*, 20.

[73] Guo, H.; Zhang, P.; Huang, S. Y.; Li, M.; Sun, G. X.; Li, J. Y.; Lin, Y.; Liu, B.; Pan, Y. Achilles' heel of single atom catalysts towards practical PEMFC application: Degradation mechanisms and regulatory strategies. *Nano Res. Energy* **2025**, *4*, e9120144.

[74] Ran, Y.; Xu, C. F.; Ji, D. Y.; Zhao, H. P.; Li, L. Q.; Lei, Y. Research progress of transition metal compounds as bifunctional catalysts for zinc-air batteries. *Nano Res. Energy* **2024**, *3*, e9120092.

[75] Jin, W.; Du, H.; Zheng, S. L.; Xu, H. B.; Zhang, Y. Comparison of the oxygen reduction reaction between NaOH and KOH solutions on a Pt electrode: The electrolyte-dependent effect. *J. Phys. Chem. B* **2010**, *114*, 6542–6548.

[76] Strmcnik, D. ; van der Vliet, D. F.; Chang, K. C.; Komanicky, V.; Kodama, K.; You, H.; Stamenkovic, V. R.; Marković, N. M. Effects of Li^+, K^+, and Ba^{2+} cations on the ORR at model and high surface area Pt and Au surfaces in alkaline solutions. *J. Phys. Chem. Lett.* **2011**, *2*, 2733–2736.

[77] Wang, T.; Zhang, Y. R.; Huang, B. T.; Cai, B.; Rao, R. R.; Giordano, L.; Sun, S. G.; Shao-Horn, Y. Enhancing oxygen reduction electrocatalysis by tuning interfacial hydrogen bonds. *Nat. Catal.* **2021**, *4*, 753–762.

[78] Li, Y. W.; Malkani, A.; Gawas, R.; Intikhab, S.; Xu, B. J.; Tang, M.; Snyder, J. Interfacial water manipulation with ionic liquids for the oxygen reduction reaction. *ACS Catal.* **2023**, *13*, 382–391.

[79] He, Q. G.; Yang, X. F.; Chen, W.; Mukerjee, S.; Koel, B.; Chen, S. W. Influence of phosphate anion adsorption on the kinetics of oxygen electroreduction on low index Pt (*hkl*) single crystals. *Phys. Chem. Chem. Phys.* **2010**, *12*, 12544–12555.

[80] Stamenkovic, V.; Markovic, N. M.; Ross, P. N. Jr. Structure-relationships in electrocatalysis: Oxygen reduction and hydrogen oxidation reactions on Pt (111) and Pt (100) in solutions containing chloride ions. *J. Electroanal. Chem.* **2001**, *500*, 44–51.

[81] Bagotzky, V. S.; Vassilyev, Y. B.; Weber, J.; Pirtskhalava, J. N. Adsorption of anions on smooth platinum electrodes. *J. Electroanal. Chem. Interfacial Electrochem.* **1970**, *27*, 31–46.

[82] Wang, Y. R.; Ding, H. M.; Yue, M.; Li, Q.; Shi, J. W.; Huang, Q.; Zhou, J.; Zang, Y.; Chen, Y. F.; Li, S. L. et al. Subtle tuning of micro-environment in COFs nanoribbons actuates low electricity-consumption photo-assisted Co-electrolysis of methanol and CO_2. *Nano Res. Energy* **2025**, *4*, e9120146.

[83] Murata, A.; Hori, Y. Product selectivity affected by cationic species in electrochemical reduction of CO_2 and CO at a Cu electrode. *Bull. Chem. Soc. Japan* **1991**, *64*, 123–127.

[84] Monteiro, M. C. O.; Dattila, F.; Hagedoorn, B.; García-Muelas, R.; López, N.; Koper, M. T. M. Absence of CO_2 electroreduction on copper, gold and silver electrodes without metal cations in solution. *Nat. Catal.* **2021**, *4*, 654–662.

[85] Ovalle, V. J.; Hsu, Y. S.; Agrawal, N.; Janik, M. J.; Waegele, M. M. Correlating hydration free energy and specific adsorption of alkali metal cations during CO_2 electroreduction on Au. *Nat. Catal.* **2022**, *5*, 624–632.

[86] Gu, J.; Liu, S.; Ni, W.; Ren, W.; Haussener, S.; Hu, X. Modulating electric field distribution by alkali cations for CO_2 electroreduction in strongly acidic medium. *Nat. Catal.* **2022**, *5*, 268–276.

[87] Bui, J. C.; Kim, C.; King, A. J.; Romiluyi, O.; Kusoglu, A.; Weber, A. Z.; Bell, A. T. Engineering catalyst-electrolyte microenvironments to optimize the activity and selectivity for the electrochemical reduction of CO_2 on Cu and Ag. *Acc. Chem. Res.* **2022**, *55*, 484–494.

[88] Monteiro, M. C. Q.; Dattila, F.; López, N.; Koper, M. T. M. The role of cation acidity on the competition between hydrogen evolution and CO_2 reduction on gold electrodes. *J. Am. Chem. Soc.* **2022**, *144*, 1589–1602.

[89] Yu, S.; Yamauchi, H.; Wang, S.; Aggarwal, A.; Kim, J.; Gordiz, K.; Huang, B. T.; Xu, H. B.; Zheng, D. J.; Wang, X. et al. CO_2-to-methanol electroconversion on a molecular cobalt catalyst facilitated by acidic cations. *Nat. Catal.* **2024**, *7*, 1000–1009.

[90] Resasco, J.; Lum, Y.; Clark, E.; Zeledon, J. Z.; Bell, A. T. Effects of anion identity and concentration on electrochemical reduction of CO_2. *ChemElectroChem* **2018**, *5*, 1064–1072.

[91] Varela, A. S.; Ju, W.; Reier, T.; Strasser, P. Tuning the catalytic activity and selectivity of Cu for CO_2 electroreduction in the presence of halides. *ACS Catal.* **2016**, *6*, 2136–2144.

[92] Kwon, Y.; Lum, Y.; Clark, E. L.; Ager, J. W.; Bell, A. T. CO_2 electroreduction with enhanced ethylene and ethanol selectivity by nanostructuring polycrystalline copper. *ChemElectroChem* **2016**, *3*, 1012–1019.

[93] Tao, H. L.; Lian, C.; Jiang, H.; Li, C. Z.; Liu, H. L.; van Roij, R. Enhancing electrocatalytic N_2 reduction via tailoring the electric double layers. *AlChE J.* **2022**, *68*, e17549.

[94] Wang, J.; Yu, L.; Hu, L.; Chen, G.; Xin, H. L.; Feng, X. F. Ambient ammonia synthesis via palladium-catalyzed electrohydrogenation of dinitrogen at low overpotential. *Nat. Commun.* **2018**, *9*, 1795.

[95] Kani, N. C.; Prajapati, A.; Collins, B. A.; Goodpaster, J. D.; Singh, M. R. Competing effects of pH, cation identity, H_2O saturation, and N_2 concentration on the activity and selectivity of electrochemical reduction of N_2 to NH_3 on electrodeposited Cu at ambient conditions. *ACS Catal.* **2020**, *10*, 14592–14603.

[96] Hao, Y. C.; Guo, Y.; Chen, L. W.; Shu, M.; Wang, X. Y.; Bu, T. A.; Gao, W. Y.; Zhang, N.; Su, X.; Feng, X. et al. Promoting nitrogen electroreduction to ammonia with bismuth nanocrystals and potassium cations in water. *Nat. Catal.* **2019**, *2*, 448–456.

[97] Ren, Y. W.; Yu, C.; Han, X. T.; Tan, X. Y.; Wei, Q. B.; Li, W. B.; Han, Y. N.; Yang, L.; Qiu, J. S. Methanol-mediated electrosynthesis of ammonia. *ACS Energy Lett.* **2021**, *6*, 3844–3850.

[98] Xu, X. L.; Song, X. J.; Liu, X. H.; Wang, H. F.; Hu, Y. F.; Xia, J.; Chen, J. C.; Shakouri, M.; Guo, Y.; Wang, Y. Q. A highly efficient nickel phosphate electrocatalyst for the oxidation of 5-hydroxymethylfurfural to 2,5-furandicarboxylic acid. *ACS Sustain. Chem. Eng.* **2022**, *10*, 5538–5547.

[99] Xia, Z. C.; Xu, L. T.; Ma, C. Y.; An, Q. Z.; Bu, C. Y.; Fan, Y.; Lu, Y. X.; Pan, Y. P.; Xie, D. K.; Liu, Q. H. et al. Enhancing the electrocatalytic hydrogenation of furfural via anion-induced molecular activation and adsorption. *J. Am. Chem. Soc.* **2024**, *146*, 24570–24579.

[100] Wu, J. X.; Li, J. L.; Li, Y. F.; Ma, X. Y.; Zhang, W. Y.; Hao, Y. M.; Cai, W. B.; Liu, Z. P.; Gong, M. Steering the glycerol electro-reforming selectivity via cation-intermediate interactions. *Angew. Chem., Int. Ed.* **2022**, *61*, e202113362.

[101] Yang, T.; Yang, J. T.; Deng, X.; Franz, E.; Fromm, L.; Taccardi, N.; Liu, Z.; Görling, A.; Wasserscheid, P.; Brummel, O. et al. Modifying the electrocatalytic selectivity of oxidation reactions with ionic liquids. *Angew. Chem. Int. Ed.* **2022**, *61*, e202202957.

[102] Sreekanth, N.; Phani, K. L. Selective reduction of CO_2 to formate through bicarbonate reduction on metal electrodes: New insights gained from SG/TC mode of SECM. *Chem. Commun.* **2014**, *50*, 11143–11146.

[103] Mariano, R. G.; McKelvey, K.; White, H. S.; Kanan, M. W. Selective increase in CO_2 electroreduction activity at grain-boundary surface terminations. *Science* **2017**, *358*, 1187–1192.

[104] Bertoncello, P. Advances on scanning electrochemical microscopy (SECM) for energy. *Energy Environ. Sci.* **2010**, *3*, 1620–1633.

[105] Kim, J.; Kim, B. K.; Cho, S. K.; Bard, A. J. Tunneling ultramicroelectrode: Nanoelectrodes and nanoparticle collisions. *J. Am. Chem. Soc.* **2014**, *136*, 8173–8176.

[106] Polcari, D.; Dauphin-Ducharme, P.; Mauzeroll, J. Scanning electrochemical microscopy: A comprehensive review of experimental parameters from 1989 to 2015. *Chem. Rev.* **2016**, *116*, 13234–13278.

[107] Izquierdo, J.; Knittel, P.; Kranz, C. Scanning electrochemical microscopy: An analytical perspective. *Anal. Bioanal. Chem.* **2018**, *410*, 307–324.

[108] Limani, N.; Boudet, A.; Blanchard, N.; Jousselme, B.; Cornut, R. Local probe investigation of electrocatalytic activity. *Chem. Sci.* **2021**, *12*, 71–98.

[109] Fernández, J. L.; Walsh, D. A.; Bard, A. J. Thermodynamic guidelines for the design of bimetallic catalysts for oxygen electroreduction and rapid screening by scanning electrochemical microscopy. M-Co (M: Pd, Ag, Au). *J. Am. Chem. Soc.* **2005**, *127*, 357–365.

[110] Ahn, H. S.; Bard, A. J. Surface interrogation of CoP_i water oxidation catalyst by scanning electrochemical microscopy. *J. Am. Chem. Soc.* **2015**, *137*, 612–615.

[111] Mayer, F. D.; Hosseini-Benhangi, P.; Sánchez-Sánchez, C. M.; Asselin, E.; Gyenge, E. L. Scanning electrochemical microscopy screening of CO_2 electroreduction activities and product selectivities of catalyst arrays. *Commun. Chem.* **2020**, *3*, 155.

[112] Strange, L. E.; Yadav, J.; Li, X.; Pan, S. L. Editors' choice-review-creating electrocatalytic heterojunctions for efficient photoelectrochemical CO_2 reduction to chemical fuels. *J. Electrochem. Soc.* **2020**, *167*, 146518.

[113] Garcia-Araez, N.; Climent, V.; Feliu, J. Potential-dependent water orientation on Pt (111), Pt (100), and Pt (110), as inferred from laser-pulsed experiments. Electrostatic and chemical effects. *J. Phys. Chem. C* **2009**, *113*, 9290–9304.

[114] Climent, V.; Coles, B. A.; Compton, R. G. Laser-induced potential transients on a Au (111) single-crystal electrode. Determination of the potential of maximum entropy of double-layer formation. *J. Phys. Chem. B* **2002**, *106*, 5258–5265.

[115] Sebastián, P.; Martínez-Hincapié, R.; Climent, V.; Feliu, J. M. Study of the Pt (111) | electrolyte interface in the region close to neutral pH solutions by the laser induced temperature jump technique. *Electrochim. Acta* **2017**, *228*, 667–676.

[116] Sebastián-Pascual, P.; Sarabia, F. J.; Climent, V.; Feliu, J. M.; Escudero-Escribano, M. Elucidating the structure of the Cu-alkaline electrochemical interface with the laser-induced temperature jump method. *J. Phys. Chem. C* **2020**, *124*, 23253–23259.

[117] Auer, A.; Ding, X.; Bandarenka, A. S.; Kunze-Liebhäuser, J. The potential of zero charge and the electrochemical interface structure of Cu (111) in alkaline solutions. *J. Phys. Chem. C* **2021**, *125*, 5020–5028.

[118] Favaro, M.; Jeong, B.; Ross, P. N.; Yano, J.; Hussain, Z.; Liu, Z.; Crumlin, E. J. Unravelling the electrochemical double layer by direct probing of the solid/liquid interface. *Nat. Commun.* **2016**, *7*, 12695.

[119] Bhattacharyya, D.; Videla, P. E.; Cattaneo, M.; Batista, V. S.; Lian, T. Q.; Kubiak, C. P. Vibrational Stark shift spectroscopy of catalysts under the influence of electric fields at electrode-solution interfaces. *Chem. Sci.* **2021**, *12*, 10131–10149.

[120] Liu, H. J.; Qi, Z. M.; Song, L. *In situ* electrocatalytic infrared spectroscopy for dynamic reactions. *J. Phys. Chem. C* **2021**, *125*, 24289–24300.

[121] Zhang, L.; Yang, X. J.; Yuan, Q.; Wei, Z. M.; Ding, J.; Chu, T. S.; Rong, C.; Zhang, Q.; Ye, Z. K.; Xuan, F. Z. et al. Elucidating the structure-stability relationship of Cu single-atom catalysts using *operando* surface-enhanced infrared absorption spectroscopy. *Nat. Commun.* **2023**, *14*, 8311.

[122] Sun, K. A.; Wu, X. Y.; Zhuang, Z. W.; Liu, L. Y.; Fang, J. J.; Zeng, L. Y.; Ma, J. G.; Liu, S. J.; Li, J. Z.; Dai, R. Y. et al. Interfacial water engineering boosts neutral water reduction. *Nat. Commun.* **2022**, *13*, 6260.

[123] Radjenovic, P. M.; Zhou, R. Y.; Dong, J. C.; Li, J. F. Watching reactions at solid-liquid interfaces with *in situ* Raman spectroscopy. *J. Phys. Chem. C* **2021**, *125*, 26285–26295.

[124] Tang, C. Y.; Wei, C.; Fang, Y. Y.; Liu, B.; Song, X. Y.; Bian, Z. N.; Yin, X. W.; Wang, H. B.; Liu, Z. H.; Wang, G. M. et al. Electrocatalytic hydrogenation of acetonitrile to ethylamine in acid. *Nat. Commun.* **2024**, *15*, 3233.

[125] Liu, Y. D.; Li, L.; Wang, L.; Li, N.; Zhao, X. X.; Chen, Y.; Sakthivel, T.; Dai, Z. F. Janus electronic state of supported iridium nanoclusters for sustainable alkaline water electrolysis. *Nat. Commun.* **2024**, *15*, 2851.

[126] Zhao, J. W.; Yue, K. H.; Zhang, H.; Wei, S. Y.; Zhu, J. W.; Wang, D. D.; Chen, J. Z.; Fominski, V. Y.; Li, G. R. The formation of unsaturated IrO_x in $SrIrO_3$ by cobalt-doping for acidic oxygen evolution reaction. *Nat. Commun.* **2024**, *15*, 2928.

[127] van Schooneveld, M. M.; Gosselink, R. W.; Eggenhuisen, T. M.; Al Samarai, M.; Monney, C.; Zhou, K. J.; Schmittde, T. ; de Groot, F. M. A multispectroscopic study of 3d orbitals in cobalt carboxylates: The high sensitivity of 2p3d resonant X-ray emission spectroscopy to the ligand field. *Angew. Chem. Int. Ed.* **2013**, *52*, 1170–1174.

[128] Cao, X. Y.; Tan, D. X.; Wulan, B.; Hui, K. S.; Hui, K. N.; Zhang, J. T. *In situ* characterization for boosting electrocatalytic carbon dioxide reduction. *Small Methods* **2021**, *5*, 2100700.

[129] Deng, Y. L.; Yeo, B. S. Characterization of electrocatalytic water splitting and CO_2 reduction reactions using *in situ*/*operando* Raman spectroscopy. *ACS Catal.* **2017**, *7*, 7873–7889.

[130] Yang, H.; Hu, Y. W.; Chen, J. J.; Balogun, M. S.; Fang, P. P.; Zhang, S. Q.; Chen, J.; Tong, Y. X. Intermediates adsorption engineering of CO_2 electroreduction reaction in highly selective heterostructure Cu-based electrocatalysts for CO production. *Adv. Energy Mater.* **2019**, *9*, 1901396.

[131] Brosseau, C. L.; Colina, A.; Perales-Rondon, J. V.; Wilson, A. J.; Joshi, P. B.; Ren, B.; Wang, X. Electrochemical surface-enhanced Raman spectroscopy. *Nat. Rev. Methods Primers* **2023**, *3*, 79.

[132] Li, J. F.; Huang, Y. F.; Ding, Y.; Yang, Z. L.; Li, S. B.; Zhou, X. S.; Fan, F. R.; Zhang, W.; Zhou, Z. Y.; Wu, D. Y. et al. Shell-isolated nanoparticle-enhanced Raman spectroscopy. *Nature* **2010**, *464*, 392–395.

[133] Zhang, H.; Duan, S.; Radjenovic, P. M.; Tian, Z. Q.; Li, J. F. Core-shell nanostructure-enhanced Raman spectroscopy for surface catalysis. *Acc. Chem. Res.* **2020**, *53*, 729–739.

[134] Deckert-Gaudig, T.; Taguchi, A.; Kawata, S.; Deckert, V. Tip-enhanced Raman spectroscopy-from early developments to recent advances. *Chem. Soc. Rev.* **2017**, *46*, 4077–4110.

[135] Verma, P. Tip-enhanced Raman spectroscopy: Technique and recent advances. *Chem. Rev.* **2017**, *117*, 6447–6466.
[136] Duan, S.; Tian, G. J.; Luo, Y. Theoretical and computational methods for tip-and surface-enhanced Raman scattering. *Chem. Soc. Rev.* **2024**, *53*, 5083–5117.
[137] Bao,Y. F.; Zhu, M. Y.; Zhao, X. J.; Chen, H. X.; Wang, X.; Ren, B. Nanoscale chemical characterization of materials and interfaces by tip-enhanced Raman spectroscopy. *Chem. Soc. Rev.* **2024**, *53*, 10044–10079.
[138] Schoonheydt, R. A. UV-VIS-NIR spectroscopy and microscopy of heterogeneous catalysts. *Chem. Soc. Rev*. **2010**, *39*, 5051–5066.
[139] Herl, T.; Matysik, F. M. Recent developments in electrochemistry-mass spectrometry. *ChemElectroChem* **2020**, *7*, 2498–2512.
[140] Bruckenstein, S.; Gadde, R. R. Use of a porous electrode for *in situ* mass spectrometric determination of volatile electrode reaction products. *J. Am. Chem. Soc.* **1971**, *93*, 793–794.
[141] Hoch, G.; Kok, B. A mass spectrometer inlet system for sampling gases dissolved in liquid phases. *Arch. Biochem. Biophys.* **1963**, *101*, 160–170.
[142] Wolter, O.; Heitbaum, J. Differential electrochemical mass spectroscopy (DEMS)-a new method for the study of electrode processes. *Ber. Bunsenges. Phys. Chem.* **1984**, *88*, 2–6.
[143] Fukui, N.; Cha, W. Y.; Lee, S.; Tokuji, S.; Kim, D.; Yorimitsu, H.; Osuka, A. Oxidative fusion reactions of meso-(diarylamino) porphyrins. *Angew. Chem., Int. Ed.* **2013**, *52*, 9728–9732.
[144] Cheng, H. Y.; Tang, S. L.; Yang, T. Y.; Xu, S. Q.; Yan, X. Accelerating electrochemical reactions in a voltage-controlled interfacial microreactor. *Angew. Chem., Int. Ed.* **2020**, *59*, 19862–19867.
[145] Gu, C. Y.; Nie, X.; Jiang, J. Z.; Chen, Z. F.; Dong, Y. F.; Zhang, X.; Liu, J. J.; Yu, Z. Y.; Zhu, Z. W.; Liu, J. et al. Mechanistic study of oxygen reduction at liquid/liquid interfaces by hybrid ultramicroelectrodes and mass spectrometry. *J. Am. Chem. Soc.* **2019**, *141*, 13212–13221.
[146] Hambitzer, G.; Heitbaum, J. Electrochemical thermospray mass spectrometry. *Anal. Chem.* **1986**, *58*, 1067–1070.
[147] Bartmess, J. E.; Phillips, L. R. Electrochemically assisted fast atom bombardment mass spectrometry. *Anal. Chem.* **1987**, *59*, 2012–2014.
[148] Smoluch, M.; Mielczarek, P.; Reszke, E.; Hieftje, G. M.; Silberring, J. Determination of psychostimulants and their metabolites by electrochemistry linked on-line to flowing atmospheric pressure afterglow mass spectrometry. *Analyst* **2014**, *139*, 4350–4355.
[149] Zhou, F. M. Electrochemistry combined on-line with atomic mass spectrometry and related techniques for trace-metal analysis and electrode-reaction studies. *TrAC Trends Anal. Chem.* **2005**, *24*, 218–227.
[150] Takáts, Z.; Wiseman, J. M.; Gologan, B.; Cooks, R. G. Mass spectrometry sampling under ambient conditions with desorption electrospray ionization. *Science* **2004**, *306*, 471–473.
[151] Benninghoven, A. Developments in secondary ion mass spectroscopy and applications to surface studies. *Surf. Sci.* **1975**, *53*, 596–625.
[152] Yamashita, M.; Fenn, J. B. Electrospray ion source. Another variation on the free-jet theme. *J. Phys. Chem.* **1984**, *88*, 4451–4459.
[153] Siegbahn, K. *ESCA Applied to Free Molecules*; North-Holland Pub. Co.: Amsterdam, 1969.
[154] Joyner, R. W.; Roberts, M. W.; Yates, K. A "high-pressure" electron spectrometer for surface studies. *Surf. Sci.* **1979**, *87*, 501–509.
[155] Siegbahn, H. Electron spectroscopy for chemical analysis of liquids and solutions. *J. Phys. Chem.* **1985**, *89*, 897–909.
[156] Littrell, D. M.; Tatarchuk, B. J. Hydrazine reduction of transition metal oxides: *In situ* characterization using X-ray photoelectron spectroscopy. *J. Vac. Sci. Technol. A* **1986**, *4*, 1608–1612.
[157] Handoko, A. D.; Wei, F. X.; Jenndy; Yeo, B. S.; Seh, Z. W. Understanding heterogeneous electrocatalytic carbon dioxide reduction through *operando* techniques. *Nat. Catal.* **2018**, *1*, 922–934.
[158] Bordiga, S.; Groppo, E.; Agostini, G. ; van Bokhoven, J. A.; Lamberti, C. Reactivity of surface species in heterogeneous catalysts probed by *in situ* X-ray absorption techniques. *Chem. Rev.* **2013**, *113*, 1736–1850.
[159] Billinge, S. J. L.; Levin, I. The problem with determining atomic structure at the nanoscale. *Science* **2007**, *316*, 561–565.
[160] Timoshenko, J.; Frenkel, A. I. "Inverting" X-ray absorption spectra of catalysts by machine learning in search for activity descriptors. *ACS Catal.* **2019**, *9*, 10192–10211.
[161] Grunwaldt, J. D.; Kimmerle, B.; Baiker, A.; Boye, P.; Schroer, C. G.; Glatzel, P.; Borca, C. N.; Beckmann, F. Catalysts at work: From integral to spatially resolved X-ray absorption spectroscopy. *Catal. Today* **2009**, *145*, 267–278.
[162] De Luna, P.; Quintero-Bermudez, R.; Dinh, C. T.; Ross, M. B.; Bushuyev, O. S.; Todorović, P.; Regier, T.; Kelley, S. O.; Yang, P. D.; Sargent, E. H. Catalyst electro-redeposition controls morphology and oxidation state for selective carbon dioxide reduction. *Nat. Catal.* **2018**, *1*, 103–110.
[163] Lee, S. H.; Lin, J. C.; Farmand, M.; Landers, A. T.; Feaster, J. T.; Avilés Acosta, J. E.; Beeman, J. W.; Ye, Y. F.; Yano, J.; Mehta, A. et al. Oxidation state and surface reconstruction of Cu under CO_2 reduction conditions from *in situ* X-ray characterization. *J. Am. Chem. Soc.* **2021**, *143*, 588–592.
[164] Zhuang, T. T.; Liang, Z. Q.; Seifitokaldani, A.; Li, Y.; De Luna, P.; Burdyny, T.; Che, F. L.; Meng, F.; Min, Y. M.; Quintero-Bermudez, R. et al. Steering post-C-C coupling selectivity enables high efficiency electroreduction of carbon dioxide to multi-carbon alcohols. *Nat. Catal.* **2018**, *1*, 421–428.
[165] Zheng, X. L.; Zhang, B.; De Luna, P.; Liang, Y. F.; Comin, R.; Voznyy, O.; Han, L. L.; García de Arquer, F. P.; Liu, M.; Dinh, C. T. et al. Theory-driven design of high-valence metal sites for water oxidation confirmed using *in situ* soft X-ray absorption. *Nat. Chem.* **2018**, *10*, 149–154.
[166] Saveleva, V. A.; Ebner, K.; Ni, L. M.; Smolentsev, G.; Klose, D.; Zitolo, A.; Marelli, E.; Li, J. K.; Medarde, M.; Safonova, O. V. et al. Potential-induced spin changes in Fe/N/C electrocatalysts assessed by *in situ* X-ray emission spectroscopy. *Angew. Chem., Int. Ed.* **2021**, *60*, 11707–11712.
[167] Zitolo, A.; Goellner, V.; Armel, V.; Sougrati, M. T.; Mineva, T.; Stievano, L.; Fonda, E.; Jaouen, F. Identification of catalytic sites for oxygen reduction in iron-and nitrogen-doped graphene materials. *Nat. Mater.* **2015**, *14*, 937–942.
[168] Bhargava, A.; Chen, C. Y.; Finkelstein, K. D.; Ward, M. J.; Robinson, R. D. X-ray emission spectroscopy: An effective route to extract site occupation of cations. *Phys. Chem. Chem. Phys.* **2018**, *20*, 28990–29000.
[169] Zimmermann, P.; Hunault, M. O. J. Y.; de Groot, F. M. F. 1s2p RIXS calculations for 3d transition metal ions in octahedral symmetry. *J. Spectrosc.* **2018**, *2018*, 3618463.
[170] Glatzel, P.; Singh, J.; Kvashnina, K. O.; van Bokhoven, J. A. *In situ* characterization of the 5d density of states of Pt nanoparticles upon adsorption of CO. *J. Am. Chem. Soc.* **2010**, *132*, 2555–2557.
[171] Mei, B. B.; Liu, C.; Li, J.; Gu, S. Q.; Du, X. L.; Lu, S. Y.; Song, F.; Xu, W. L.; Jiang, Z. *Operando* HERFD-XANES and surface sensitive $\Delta\mu$ analyses identify the structural evolution of copper (II) phthalocyanine for electroreduction of CO_2. *J. Energy Chem.* **2022**, *64*, 1–7.
[172] Williamson, M. J.; Tromp, R. M.; Vereecken, P. M.; Hull, R.; Ross, F. M. Dynamic microscopy of nanoscale cluster growth at the solid-liquid interface. *Nat. Mater.* **2003**, *2*, 532–536.
[173] Zheng, H. M.; Smith, R. K.; Jun, Y. W.; Kisielowski, C.; Dahmen, U.; Alivisatos, A. P. Observation of single colloidal platinum nanocrystal growth trajectories. *Science* **2009**, *324*, 1309–1312.
[174] Liao, H. G.; Zherebetskyy, D.; Xin, H. L.; Czarnik, C.; Ercius, P.;

Elmlund, H.; Pan, M.; Wang, L. W.; Zheng, H. M. Facet development during platinum nanocube growth. *Science* **2014**, *345*, 916–919.
[175] Liao, H. G.; Cui, L. K.; Whitelam, S.; Zheng, H. M. Real-time imaging of Pt_3Fe nanorod growth in solution. *Science* **2012**, *336*, 1011–1014.
[176] Wang, X. L.; Klingan, K.; Klingenhof, M.; Möller, T.; Ferreira de Araújo, J.; Martens, I.; Bagger, A.; Jiang, S.; Rossmeisl, J.; Dau, H. et al. Morphology and mechanism of highly selective Cu (II) oxide nanosheet catalysts for carbon dioxide electroreduction. *Nat. Commun.* **2021**, *12*, 794.
[177] Li, J.; Johnson, G.; Zhang, S.; Su, D. *In situ* transmission electron microscopy for energy applications. *Joule* **2019**, *3*, 4–8.
[178] Lei, Q.; Zhu, H.; Song, K. P.; Wei, N. N.; Liu, L. M.; Zhang, D. L.; Yin, J.; Dong, X. L.; Yao, K. X.; Wang, N. et al. Investigating the origin of enhanced C_{2+} selectivity in oxide-/hydroxide-derived copper electrodes during CO_2 electroreduction. *J. Am. Chem. Soc.* **2020**, *142*, 4213–4222.

Xianwei Liu is currently pursuing his doctor's degree under the supervision of Professor Chuangang Hu and Associate Professor Baoguang Mao at the College of Chemical Engineering, Beijing University of Chemical Technology. He received his bachelor's degree in chemical engineering and technology from Beijing University of Chemical Technology in 2021. His research interests focus on the design of OER ruthenium-based catalysts and the optimization of PEMWE devices.

Xianrong Zhang is currently pursuing her master's degree under the supervision of Associate Professor Baoguang Mao at the College of Chemical Engineering, Beijing University of Chemical Technology. She received her bachelor's degree in Chemical Engineering and Technology from Shandong University of Science and Technology in 2024. Her research interest focuses on ethylene glycol oxidation reaction.

Yuanqing Shen is currently pursuing his master's degree under the supervision of Professor Chuangang Hu at the College of Chemical Engineering, Beijing University of Chemical Technology. He received his bachelor's degree in chemical engineering and technology from Beijing University of Chemical Technology in 2025. His research interests focus on small molecule electrocatalysis of carbon-based materials.

Linjie Zhao works as a postdoctoral researcher at the College of Chemical Engineering, Beijing University of Chemical Technology. He received his doctor's degree in chemical engineering and technology from Beijing University of Chemical Technology in 2024. His research interests focus on specially designed carbon-based materials for energy conversion and storage.

Baoguang Mao is an associate professor at the College of Chemical Engineering, Beijing University of Chemical Technology. He received his MS from Tiangong University in 2014, and his PhD from Beijing Institute of Technology in 2018. He worked as a postdoctoral researcher at Beijing Institute of Technology from 2020 to 2022. His research interests focus on energy electrocatalysis and electrode/electrolyte interfaces involved in electrochemical process.

Chuangang Hu is a professor at the College of Chemical Engineering, Beijing University of Chemical Technology. He received his MS from Henan Normal University in 2011, and his PhD from Beijing Institute of Technology in 2015. After receiving PhD degree, he continued his postdoctoral studies for 5 years at Case Western Reserve University (4 years), USA and the University of New South Wales (1 year), Australia. His research interests focus on the design and preparation of advanced carbon-based materials for environmental remediation, energy conversion, and storage.